FEDERAL UNIVERSITY OF UBERLANDIA
SCHOOL OF MECHANICAL ENGINEERING
MECHANICAL ENGINEERING GRADUATE PROGRAM

RAIMUNDO ARRAIS DE OLIVEIRA NETO

NUMERICAL MODELING OF MAGNETORHEOLOGICAL DAMPERS: A NEURO-FUZZY APPROACH

UBERLANDIA
2021

RAIMUNDO ARRAIS DE OLIVEIRA NETO

NUMERICAL MODELING OF MAGNETORHEOLOGICAL DAMPERS: A NEURO-FUZZY APPROACH

Thesis submitted to the Mechanical Engineering Graduate Program at the Federal University of Uberlandia, as part of the necessary requirements to obtain the degree of Master of Science in Mechanical Engineering.

Concentration Area: Solid Mechanics and Vibrations

Professor Advisor: Dr. Aldemir Aparecido Cavalini Junior

UBERLANDIA
2021

Ficha Catalográfica Online do Sistema de Bibliotecas da UFU
com dados informados pelo(a) próprio(a) autor(a).

O48 Oliveira Neto, Raimundo Arrais de, 1993-
2021 Numerical modeling of magnetorheological dampers [recurso eletrônico] : a neuro-fuzzy approach / Raimundo Arrais de Oliveira Neto. - 2021.

Orientador: Aldemir Aparecido Cavalini Junior.
Dissertação (Mestrado) - Universidade Federal de Uberlândia, Pós-graduação em Engenharia Mecânica.
Modo de acesso: Internet.
Disponível em: http://doi.org/10.14393/ufu.di.2021.361
Inclui bibliografia.
Inclui ilustrações.

1. Engenharia mecânica. I. Cavalini Junior, Aldemir Aparecido ,1983-, (Orient.). II. Universidade Federal de Uberlândia. Pós-graduação em Engenharia Mecânica. III. Título.

CDU: 621

Bibliotecários responsáveis pela estrutura de acordo com o AACR2:

Gizele Cristine Nunes do Couto - CRB6/2091

UNIVERSIDADE FEDERAL DE UBERLÂNDIA
Coordenação do Programa de Pós-Graduação em Engenharia Mecânica
Av. João Naves de Ávila, nº 2121, Bloco 1M, Sala 212 - Bairro Santa Mônica, Uberlândia-MG, CEP 38400-902
Telefone: (34) 3239-4282 - www.posgrad.mecanica.ufu.br - secposmec@mecanica.ufu.br

ATA DE DEFESA - PÓS-GRADUAÇÃO

Programa de Pós-Graduação em:	Engenharia Mecânica				
Defesa de:	Dissertação de Mestrado Acadêmico, nº 590, COPEM				
Data:	16/07/2021	Hora de início:	09:00	Hora de encerramento:	11:30
Matrícula do Discente:	11912EMC017				
Nome do Discente:	Raimundo Arrais de Oliveira Neto				
Título do Trabalho:	Numerical Modeling of Magnetorheological Dampers: a Neuro-Fuzzy Approach				
Área de concentração:	Mecânica dos Sólidos e Vibrações				
Linha de pesquisa:	Dinâmica de Sistemas Mecânicos				
Projeto de Pesquisa de vinculação:					

Reuniu-se por meio de webconferência a Banca Examinadora, designada pelo Colegiado do Programa de Pós-graduação em Engenharia Mecânica, assim composta: Professores Doutores: Valder Steffen Júnior - FEMEC/UFU; Edson Hideki Koroishi - UTFPR; e Aldemir Aparecido Cavalini Júnior - FEMEC/UFU, orientador do candidato. Ressalta-se que os Prof. Valder Steffen Júnior, Aldemir Aparecido Cavalini Júnior e o Discente participaram da defesa por meio de webconferência desde a cidade de Uberlândia/MG, Prof. Edson Hideki Koroishi desde a cidade de Cornélio Procópio/PR, em atendimento a Portaria nº 36, de 19 de março de 2020, da Coordenação de Aperfeiçoamento de Pessoal de Nível Superior - CAPES.

Iniciando os trabalhos o presidente da mesa, Dr. Aldemir Aparecido Cavalini Júnior, apresentou a Comissão Examinadora e o candidato, agradeceu a presença do público, e concedeu ao Discente a palavra para a exposição do seu trabalho. A duração da apresentação do Discente e o tempo de arguição e resposta foram conforme as normas do Programa.

A seguir o senhor(a) presidente concedeu a palavra, pela ordem sucessivamente, aos(às) examinadores(as), que passaram a arguir o(a) candidato(a). Ultimada a arguição, que se desenvolveu dentro dos termos regimentais, a Banca, em sessão secreta, atribuiu o resultado final, considerando o(a) candidato(a):

Aprovado.

Esta defesa faz parte dos requisitos necessários à obtenção do título de Mestre.

O competente diploma será expedido após cumprimento dos demais requisitos, conforme as normas do Programa, a legislação pertinente e a regulamentação interna da UFU.

Nada mais havendo a tratar foram encerrados os trabalhos. Foi lavrada a presente ata que após lida e achada conforme foi assinada pela Banca Examinadora.

Documento assinado eletronicamente por **Aldemir Aparecido Cavalini Junior**, **Professor(a) do Magistério Superior**, em 16/07/2021, às 10:58, conforme horário oficial de Brasília, com fundamento no art. 6º, § 1º, do Decreto nº 8.539, de 8 de outubro de 2015.

Documento assinado eletronicamente por **Edson Hideki Koroishi**, **Usuário Externo**, em 16/07/2021, às 10:58, conforme horário oficial de Brasília, com fundamento no art. 6º, § 1º, do Decreto nº 8.539, de 8 de outubro de 2015.

Documento assinado eletronicamente por **Valder Steffen Junior**, **Professor(a) do Magistério Superior**, em 16/07/2021, às 10:59, conforme horário oficial de Brasília, com fundamento no art. 6º, § 1º, do Decreto nº 8.539, de 8 de outubro de 2015.

A autenticidade deste documento pode ser conferida no site https://www.sei.ufu.br/sei/controlador_externo.php?acao=documento_conferir&id_orgao_acesso_externo=0, informando o código verificador **2911776** e o código CRC **29A1DCF0**.

I dedicate this work to my mom, Helena,

and to my aunt Aouda (in memoriam).

ACKNOWLEDGEMENTS

I am not where I am just on my own merit. I owe my achievements to many people, without whom I would not have been successful.

To my family, for their support at all times. Especially to these women: Helena, Margarida, Gina, Eveline, Raíza, and Júlia.

To Francisco Renan de Moura Dias, undergraduate fellow friend, for opening my eyes to the possibility of studying in Uberlandia.

To Guilherme Ramalho, for facilitating my adaptation in Uberlandia with valuable advices about the city and the university.

To Marcelo Fernandes, for his friendship and loyalty. You are my first friend in Uberlandia and you are family to me.

To Daniel Lázaro, Luiz Carlos, Jackson Vasconcelos, and José Valdenir, friends from the Military School of the Fire Department, for the support in the initial months of this journey. It is a great honor to have your friendship!

To Prof. Dr. Valder Steffen Junior, for his willingness to be available on my arrival at UFU even being in front of the university's rectory, and for accepting to be a part of the examination board.

To my advisor, Prof. Dr. Aldemir Aparecido Cavalini Junior, for his immense willingness to break barriers to do cutting edge research in Brazil and for all the support he gave me. Your attitude inspired me a lot.

To Prof. Dr. Edson Hideki Koroishi, for accepting to be a part of the examination board and for being an inspiration with his resilience.

To Prof. Dr. Rômulo do Nascimento Rodrigues, Prof. Dr. Pierre Maurice Christophe Lamary (*in memoriam*), and Prof. Dr. Roberto de Araújo Bezerra, advisor of my undergraduate final project and members of my undergraduate examination board, respectively; for believing in my potential and always encouraging me to pursue a master's degree.

To Gabriel de Melo Alves Martins and Philippe César Fernandes Teixeira for their friendship and contributions to the research developed in this work.

To the Northeastern friends at UFU: Fernanda Beatriz (Apodi/RN), Erivaldo Nunes (Bonito/PE), Gutembergy Diniz (Mossoró/RN), Marcelo Delgado (Natal/RN), and Prince Nogueira (Mossoró/RN). Your friendship made the homesickness hurt less. I will be forever grateful.

To the band friends Ely Queiroz Gomes (MSc), Alejandro Portillo (MSc), Daniel Dall'Onder (PhD), and Vitor Taha (MSc). It was nice to be studying at a master's program and be the member with the lowest degree in a rock band. Great times!

To Linda Oster, for helping me with grammatical issues.

To FAPEMIG, for the financial support with the maintenance of the scholarship.

To all the friends with whom I had the honor to talk, study or share moments together. Especially to: Higor Luís, Bruno Rende, Fernanda Rossi, João Pedro, Daniel Ferreira, Felipe do Carmo, Tatiane Nunes, Leandro Soares, Felipe dos Anjos, Antônio Lázaro, Fabrício Vieira, and Gabriella Garcia.

Thank you!

"It has to start somewhere, it has to start sometime, what better place than here? What better time than now?"

– Rage Against the Machine

OLIVEIRA NETO, R. A. **Numerical Modeling of Magnetorheological Dampers: a Neuro-Fuzzy Approach.** Master's thesis. Federal University of Uberlandia: Uberlandia, 2021.

ABSTRACT

Magnetorheological dampers are able to adapt their mechanical properties when subjected to a magnetic field which makes them a versatile option for controlling vibration in a vast number of industrial applications. This work proposes a numerical model of magnetorheological dampers using fuzzy sets as an alternative to the parametric models existing in the literature. Its main advantage is that it does not depend on highly complex mathematical modeling to represent the dynamic phenomena intrinsic to the system. Experimental data from tests previously performed with a LORD brand damper, model RD-8040-1, was used. A study of the modified Bouc-Wen Model and the Hysteretic Model was performed. Its parameters were updated by using the Differential Evolution algorithm. Then, the non-parametric model, based on neuro-fuzzy, was proposed. Through a comparison between the models, it was possible to confront the results of each model and observe that the fuzzy model was able to represent the damper in different conditions of electric current.

Keywords: Smart Materials. Neuro-Fuzzy. Magnetorheological Dampers.

OLIVEIRA NETO, R. A. **Modelagem de Amortecedores Magnetorreológicos: uma abordagem usando *neuro-fuzzy*.** Dissertação de Mestrado. Universidade Federal de Uberlândia: Uberlândia, 2021.

RESUMO

Amortecedores magnetorreológicos são capazes de adaptar suas propriedades mecânicas quando submetidos a um campo magnético, sendo, assim, uma opção versátil ao controle de vibração em diversas aplicações industriais. Este trabalho tem como objetivo propor uma modelagem de atuadores de fluido magnetorreológico utilizando lógica *fuzzy*. Essa abordagem se apresenta como uma alternativa aos modelos paramétricos existentes na literatura. Sua principal vantagem é a não dependência de uma modelagem de grande complexidade para representar os fenômenos dinâmicos intrínsecos ao sistema. Para tanto, utilizou-se dados experimentais de um experimento previamente realizado com um atuador da marca LORD modelo RD-8040-1. Foi feito um estudo dos modelos paramétricos de Bouc-Wen Modificado e do Modelo Histerético, cujos parâmetros foram ajustados utilizando o algoritmo de Evolução Diferencial. Em seguida, o modelo não paramétrico, baseado em *neuro-fuzzy*, foi proposto. Por meio de uma comparação entre os modelos, foi possível confrontar as peculiaridades de cada modelo e observar que o modelo *fuzzy* foi capaz de representar o atuador em diferentes condições de corrente elétrica.

Palavras-chave: Materiais Inteligentes. *Neuro-Fuzzy*. Amortecedores Magnetorreológicos.

Acronyms

AFC	Active Fiber Composites
ANFIS	Adaptive Neuro-Fuzzy Inference Systems
ANN	Adaptive Neural Networks
DE	Differential Evolution
EMI	Electromechanical Impedance
ER	Electrorheological
FIS	Fuzzy Inference Systems
FRBS	Fuzzy Rule-Based Systems
INCT-EIE	Nacional Institute of Science and Technology of Smart Structures in Engineering
LMEst	Laboratory of Mechanics and Structures
MF	Membership Functions
MFMS	Multifunctional Material Systems
MR	Magnetorheological
PZT	Lead Zirconate Titanate
SMA	Shape Memory Alloys
SHM	Structural Health Monitoring
UFU	Federal University of Uberlandia

List of Figures

List of Tables

CONTENTS

CHAPTER I

INTRODUCTION

"Intelligence is the ability to adapt to change."

– Unknown author

1.1 Overview

Smart materials are those that can have physical characteristics controlled by changing environmental or operational parameters, such as stress, temperature, electric or magnetic field, for example. This kind of technology opens up a wide range of possibilities. From orthodontic wires to smart structures, there are countless applications of smart materials, what motivated the Brazilian government to finance a special department of research on this field: the Nacional Institute of Science and Technology of Smart Structures in Engineering (INCT-EIE). This is a network that highlights the importance of this research field to the country and abroad.

Such institute divides the research on smart materials in seven main lines, which can give the reader an understanding about some specificities of this large field of research. The first line is related to shape memory alloys (SMA). These materials can recover their original shape, after being deformed, when a thermal load is applied. The commercial development of this technology started with pipe coupling, orthodontic wires and some medical applications in the early 1960's (SCHWARTZ, 2002). A significant number of patents were registered in this line of research in the past decade. For example, a measurement system using thermoelectric effect was patented by Araújo; Monteiro; Reis (2015). This system aimed to characterize the thermal hysteresis of SMAs by subjecting the material to electric currents on Peltier cells.

The second line deals with robust control and energy generation using smart materials. The possibility to harvest energy to provide power supply to micro-power devices motivates the development of numerous ingenious techniques in this context. Piezoelectric

materials (PZTs), for example, generate an electric charge when mechanically deformed. This characteristic enables using PZTs for energy harvesting and as sensors. For piezoelectric harvesters, the idea is to use these materials instead of the traditional batteries as power source for wireless systems. This procedure avoids the expensive battery changes and the consequent environmental problems (DORIA, 2019). For control purposes, these materials have interesting applications since a deformation causes electric charges that can be processed and interpreted numerically.

The third line deals with applications of smart materials in aeroelastic control. When elastic bodies are subjected to a fluid flow, some interactions between aerodynamic forces and the structure occur. These interactions are the field of study of aeroelasticity (HODGES; PIERCE, 2011). Understanding and controlling such interactions is of interest especially to the aeronautical industry. In this context, smart materials are mainly applied in adaptative structures to improve aircraft performance.

The fourth line of research is a subset of the third one. It is related to aeroelastic control using active fiber composites (AFCs). Such materials consist of uniaxially oriented piezoelectric fibers embedded in a polymer matrix and sandwiched between two interdigitated electrodes that polarize the fibers. When the electrodes are subjected to electric current, the electric field causes an extension on the fibers' longitudinal direction (KORNMANN, 2004). The material's ability to change its length is used to control vibrations caused by aeroelastic forces.

The fifth line of research is vibration control using smart materials. Vibration control is a classical problem in mechanical engineering. The oscillations caused in machines and structures can generate undesired effects, such as noise, wear and fatigue. Aiming to attenuate vibrations, engineers seek solutions, and smart materials are a feasible technical possibility. Some systems operate in variable conditions and it is interesting to have the ability to adapt to different situations. In this scenario, electrorheology and magnetorheology emerge with alternatives to servomechanisms and regular actuators. SMAs and smart composites are also used for the purpose of attenuating vibrations.

The sixth line is about multifunctional structures for autonomous aircrafts. Multifunctional Material Systems (MFMS) are defined as systems that integrate more than one function of different components in themselves (FERREIRA; NÓVOA; MARQUES, 2016). For example, sensing, conducting electricity, reducing drag, and structural function at the same time, thus forming multiphysics design. These systems use composite materials to achieve their

objectives. Applying that concept to aircrafts structures makes possible to reduce the number of parts and the weight, what is very interesting from the aeronautical engineering perspective.

The seventh line of research deals with smart rotors and integrity monitoring of metallic and composite structures. Indeed, the traditional inspection procedures require stopping the equipment operation, what limits the production. Thus, researchers look up for solutions that are as reliable as the traditional ones, but do not require pauses for inspection. In this sense, alternatives are sought for the prediction and prevention of failures, as well as ways to extend the useful life of the equipment, giving rise to modern Structural Health Monitoring (SHM) techniques. For example, the method of monitoring cross cracks using electromechanical impedance (EMI) technique proposed by Cavalini Júnior (2013). Likewise, Franco (2009) developed a SHM technique using piezoelectric materials as actuators and sensors based on Lamb waves. Furthermore, a failure, depending on the situation, could mean huge financial loss or, even worse, could cause deaths.

1.2 Scientific Object

This work is inserted on vibration control using smart materials, refering to the fifth line of research previously mentioned. More specifically, mathematical modeling of magnetorheological (MR) dampers, whose results help the development of alternatives to attenuate vibrations in mechanical systems. Vibration control systems are typically classified as either active or passive. Active systems employ servomechanisms to apply or absorb energy. Koroishi (2013) studied active vibration control using electromagnetic actuators on flexible shafts. Marangoni (2020) used electromagnetic actuators for active vibration control with the self-sensing technique, which does not require position sensors since the controller uses current and voltage present in the coil to perform the control action.

Passive systems consist of applying energy absorbers with fixed configurations in order to achieve certain pre-established mechanical properties, such as springs and pneumatic or hydraulic actuators. This method is relatively simple; however, the performance level is limited once the system is not able to adapt to different situations. This type of control is useful in contexts where the equipment will be subjected to a constant work regime and does not need to adapt during operation.

Despite the better performance achieved by active suspensions compared to passive suspensions, the high costs, complexity and weight overcome the advantages of that type of system, whose use is justified only in cases where performance is a critical factor (KARNOPP,

1974). Thus, Karnopp (1974) proposed a semi-active control system that combines the simplicity of passive systems with the good performance of active systems, requiring only signal processing and low levels of energy demand. Since then, many models of semi-active control systems have been developed, using electrorheological (ER) and magnetorheological (MR) dampers. Such actuators contain fluids that change their rheological properties when subjected to electric and magnetic fields, respectively. MR dampers offer low energy consumption, robustness and mechanical simplicity, which motivates several researchers to investigate their performance in structural applications (DYKE, 1996).

Figure 1.1 shows a performance comparison between active, passive and semi-active systems taken from a Lord© catalog, a major manufacturer of MR dampers and MR fluids. This is an illustration of the range of velocities for which a given damping force can be obtained. The black curve refers to passive systems, with limited scope, being designed for specific conditions and reaching maximum force only at high velocities. The gray area represents other types of suspension, including active, which modify its characteristics through controllable valves. The blue part refers to MR dampers. In this case, the velocity response at the maximum damping force is higher as compared to the others. This characteristic added to the advantages already mentioned makes this type of system quite attractive regarding practical applications.

Figure 1.1 – Performance comparison of suspension types

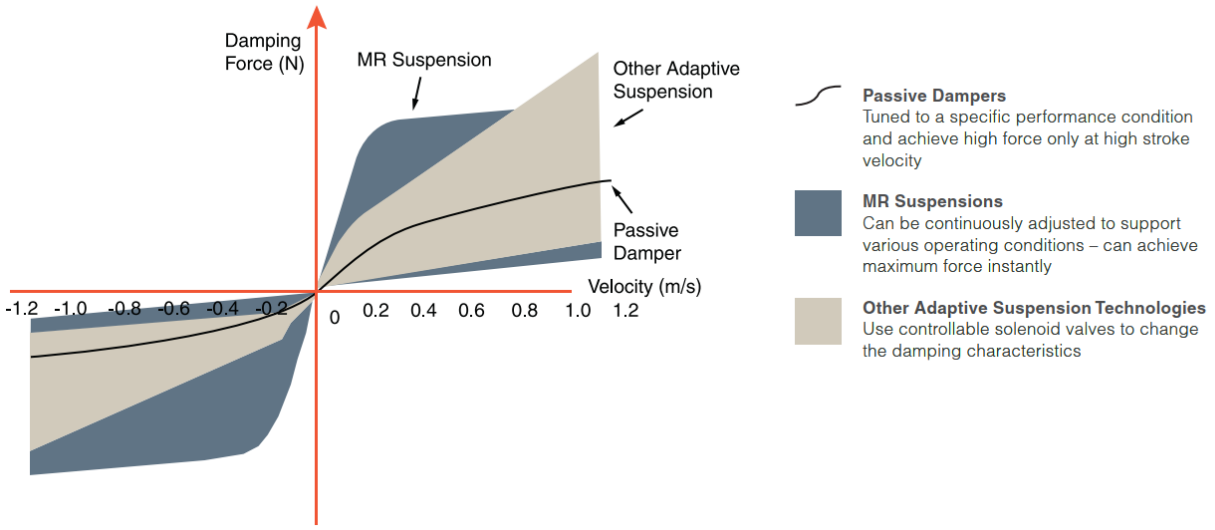

Source: Lord ([201-])

Figure 1.2 shows some MR dampers available on the market. These devices have been applied in the development of smart structures, such as bridges and buildings with

protection systems against earthquakes. Figure 1.3 illustrates applications of MR dampers in constructions. On the left, the Sanwa Tekki building is depicted, and on the right, the bridge under Dongting Lake in China is shown.

Figure 1.2 – Commercially available MR dampers

Source: Lord ([201-])

Figure 1.3 – MR dampers in buildings

Source: Liu; Tomizuka; Ulsoy (2006).

Another important application is in the automotive sector, where semi-active control allows for the suspension system to adapt to lane variations, obtaining optimal performances for vehicles suspension systems, more comfort and safety for users (PASCHOAL, 2011). An example of comfort products designed by using MR dampers is

shown in Figure 1.4. A vehicle seat that adapts its stiffness depending on track conditions, relieving the impacts on the passenger's body.

There are countless mathematical models of MR dampers. Usually, the models are parametric and non-parametric models. Parametric models are based on mathematical expressions with parameters to be adjusted to represent the MR damper. Non-parametric models are based on approaches that do not require the parameter fitting, such as the model created by using fuzzy logic. This work analyses the differences between parametric models and proposes a non-parametric alternative model by using fuzzy sets.

Figure 1.4 – Seat suspension system

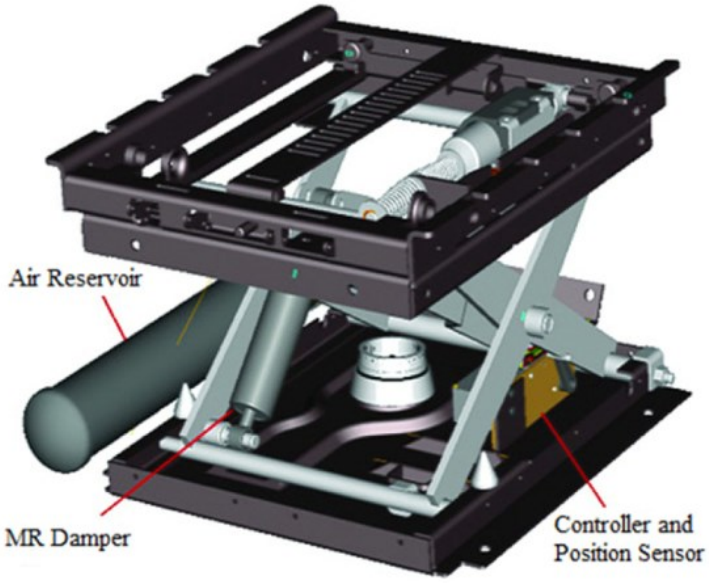

Source: Jim Toscano (2009) *apud* Ahamed; Choi; Ferdaus (2018)

According to Simões, Shaw (2007), the need to represent inaccurate quantities in a systematic way favored the advent of fuzzy logic. In fuzzy systems, modeling is defined by means of linguistic rules instead of binary propositions. This fact makes the development of this type of models extremely fast. Fuzzy systems are considered as being intelligent due to the ability to provide answers without depending only on an input value in their transfer function. The objective of studying these systems is to allow for machines to make more complex decisions, similar to human reasoning, giving more autonomy to the processes.

Schurter, Roschke (2000) developed a fuzzy model of a magnetorheological damper using ANFIS, an application developed by Mathworks© to implement adaptative neuro-fuzzy inference systems. These authors used data from a parametric model to generate the

training and checking data. The model was considered valid and showed some advantages when compared to parametric models. For example, the fuzzy approach to characterize MR dampers does not require solving multiple simultaneous differential equations.

Paschoal (2011) used a fuzzy controller in a magnetorheological damper to attenuate vibrations in vehicle suspensions. The choice of this type of controller is justified by the nonlinearities existing in this type of actuator, which has properties of different domains influencing its dynamic response. Teixeira (2017) studied some of the existing parametric models of MR fluid, developed a fuzzy model to describe the phenomena existing in the MR damper and made a comparison between parametric and non-parametric models. The major difficulty faced by that author in non-parametric modeling was the number of factors and their respective contributions to the fuzzy model, which demanded a high computational cost.

In view of this, it can be observed that the research on smart materials is very broad and promising with several ramifications of relevance. This work is focused specifically on mathematical modeling of MR dampers, whose results can be used as technical alternatives in vibration control. An investigation on different models and their performances is done. The steps followed during the development of this work and the text organization are summarized next.

1.3 Objectives and Methodology

This work has as main goal to present an alternative model of magnetorheological fluid dampers. To this goal, the following steps were performed:

- Two parametric models were adjusted, analyzed and compared;
- The fuzzy model was proposed and compared to the previous studied models;
- Data from a previous experimental characterization, executed on a MTS Landmark® testing bench using a LORD damper model RD-8040-1, was used.

1.4 Text structure

This dissertation is organized in five chapters in order to gradually provide an understanding of the theme, the relevance of the work, its theoretical foundation and application. The chapters are divided as follows.

In Chapter 1, a brief overview of the context of research on smart materials was presented. Papers from the literature were referenced forming the basis for the present thesis. The methodology used was highlighted as well as the main motivation of this work.

In Chapter 2, an extensive bibliographic research is carried out on magnetorheological dampers, magnetorheological fluid and the development of mathematical models over the years.

In Chapter 3, theoretical aspects of fuzzy logic required for the correct understanding of this work are revised.

In Chapter 4, Modified Bouc-Wen and Hysteretic models were analyzed. Numerical simulations were executed by varying the associated parameters. Some particularities of each model could be observed. Furthermore, the fuzzy model is presented and a similar analysis is made. Such a model was capable of predicting the dynamic behavior of the MR damper.

In Chapter 5, a discussion on the obtained results is performed. The conclusions and contributions of this work are presented, and perspectives of future works are briefly outlined.

CHAPTER II

MAGNETORHEOLOGICAL FLUID DAMPERS

"It's not stress that kills us, it is our reaction to it."

– Hans Selye

2.1 Introduction

MR dampers consist of a piston in a metal housing filled with MR fluid. The piston has annular holes through which the fluid passes. The main difference between MR dampers and regular dampers, other than the presence of MR fluid instead of mineral oil, is the MR piston. It has a coil which induces a magnetic field when subjected to an electric current from the power supply wires. The magnetic field changes the properties of the fluid passing through the magnetic flux region. Figure 2.1 shows the constituent parts of a MR damper assembly. The diaphragm acts as a spring to push the piston back to its steady position.

MR fluid is a mix of particles with diameters between 0.5 and 10 μm suspended in an oil. When an electric current is applied, these particles align themselves in the direction of the magnetic field (TEIXEIRA, 2017). The greater the intensity of the magnetic field, the greater the resistance of the fluid to the piston movement. Hence the semi-active characteristic of this type of device, since it acts by changing mechanical properties during operation. Figure 2.2 illustrates the alignment behavior of ferromagnetic particles in the direction of the magnetic field. The part (a) corresponds to the situation in which the fluid is not in the presence of a magnetic field, and the part (b) is when the fluid is under action of a magnetic field represented by the red arrows. Without the presence of a magnetic field, MR dampers behave like conventional dampers.

Figure 2.1 – Typical assembly of a MR damper

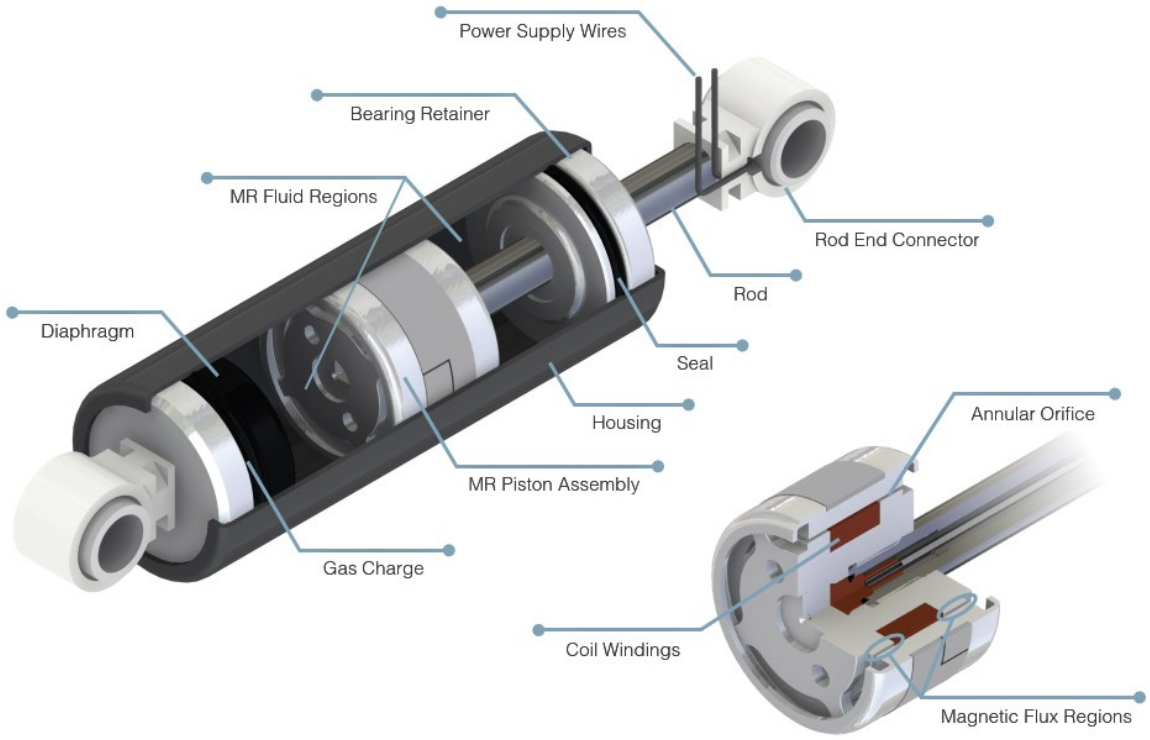

Source: Lord, ([201-])

Figure 2.2 – MR Fluid

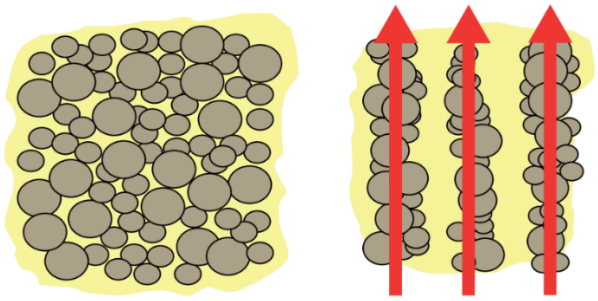

(a) magnetic field off (b) magnetic field on

Source: Lord, ([201-]).

It is quite complicated to accurately describe all the phenomena present in a magnetorheological fluid damper, since these phenomena are coupled electromagnetically, thermodynamically and hydrodynamically. Thus, simplifications of these phenomena are made (CRIVELLARO, 2008). The modeling of MR fluid can be done in two different approaches: one in the macrogeometric domain (volumes with dimensions greater than 50 μm), in which the Bingham number is used; and the other approach is in the particle domain, based in the Mason number. These numbers (Bingham and Mason) are ratios of properties that govern

equations related to the respective modeling approaches. In the macrogeometric analysis, the fluid is considered as a continuous mass with rheological properties, while in the microgeometric analysis the behavior of the suspended particles is considered, since their size is significant in such scale (SHERMAN; BECNEL; WERELEY, 2015).

2.2 Bingham Model

The Bingham viscoplastic model is usually adopted to describe the stress-strain behavior of magnetorheological and electroreological fluids (DYKE, 1996). For positive values of shear rate, the total stress is given by

$$\tau = \tau_y + \mu \cdot \dot{\gamma} \tag{2.1}$$

where τ_y represents the shear stress induced by the magnetic field, μ is the plastic viscosity, and $\dot{\gamma}$ represents the shear rate. In this model, the viscosity is given by the inclination of the shear stress caused by the field. The first right hand side term of the Equation 2.1 represents the magnetic part since it is the only part under influence of the magnetic field. The second right hand side term of that equation is the rheological part, because viscosity is independent from the magnetic field. That modeling explains the increase of shear stress when the intensity of the magnetic field is increased, as is shown in Figure 2.3.

Figure 2.3 – Shear Stress versus Shear Rate

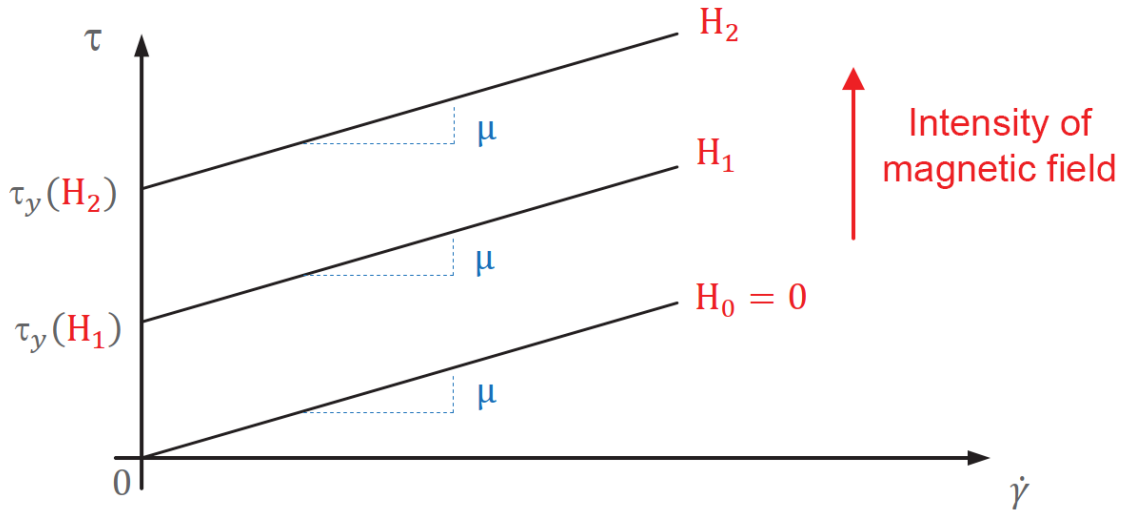

Adapted from: Srinivasan; Mcfarland (2001) *apud* Paschoal (2011)

From Bingham's plastic, Stanway, Sproston, and Stevens (1987) developed a mechanical model to predict the damping force of electrorheological dampers. The model consists of Coulomb friction in parallel with viscous damping. The model is known as Bingham Model and Figure 2.4 demonstrates it schematically.

Figure 2.4 – Bingham Model

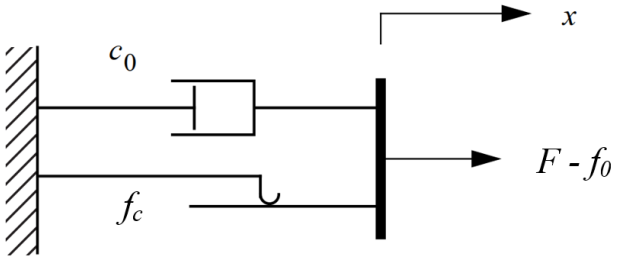

Adapted from: Dyke (1996)

Equation 2.2 describes the damping force F for non-zero velocities, whose parameters f_c, c_0, and f_0 correspond to Coulomb friction force, viscous damping, and residual force present in the diaphragm, respectively. The dependence of the movement direction is represented by $sign(\dot{x})$.

$$F = f_c \cdot sign(\dot{x}) + c_0\dot{x} + f_0 \tag{2.2}$$

Bingham Model is able to reasonably describe the force behavior versus displacement. Although, due to its simplicity, the model fails to predict the inherent transient behavior of this type of device, characterized by the hysteresis curve when changing the direction of speed (PASCHOAL, 2011).

2.3 Modified Bingham Model

In order to improve Bingham Model's performance, Gamota, and Filisko (1991) proposed a modification focusing on ER dampers. The modification consists of adding a viscoelastic-plastic model in series with the previous model. Figure 2.5 schematically illustrates the Modified Bingham model.

Figure 2.5 – Modified Bingham Model

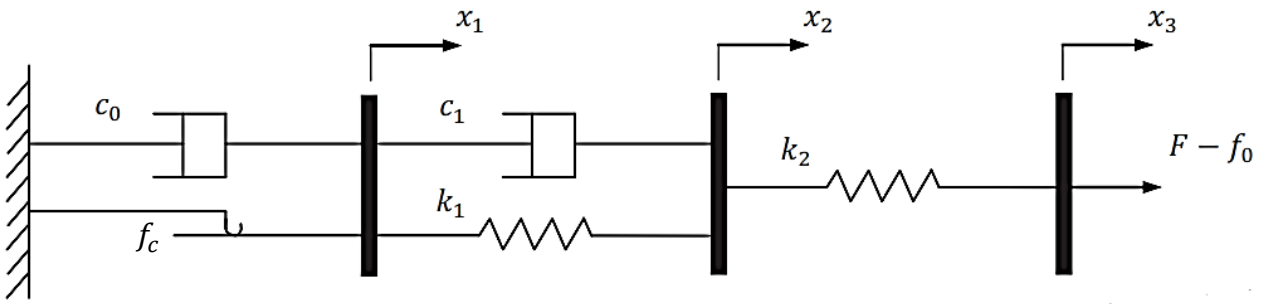

Source: Dyke (1996)

This model is governed by Equations 2.3 and 2.4, where F is the damping force, c_0 is the damping related to the Bingham model, c_1 is the viscous damping coefficient, and k_1 and k_2 are elastic stiffness constants. The parameter f_0 is the residual force present in the diaphragm and f_c represents the Coulomb frictional force. The coefficients x_1, x_2, and x_3 are displacements and $\dot{x}_1$, $\dot{x}_2$, and $\dot{x}_3$ are velocities. Moreover, when the damping force module is less than or equal Coulomb frictional force, $\dot{x}_1 = 0$ (DYKE, 1996).

$$If\ |F| > f_c, \begin{cases} F = k_1(x_2 - x_1) + c_1(\dot{x}_2 - \dot{x}_1) + f_0 \\ \quad = c_0\dot{x}_1 + f_c sign(\dot{x}_1) + f_0 \\ \quad = k_2(x_3 - x_2) + f_0 \end{cases} \tag{2.3}$$

$$If\ |F| \leq f_c, \begin{cases} F = k_1(x_2 - x_1) + c_1\dot{x}_2 + f_0 \\ \quad = k_2(x_3 - x_2) + f_0 \end{cases} \tag{2.4}$$

Dyke (1996) demonstrates that this model is able to represent a hysteresis curve, unlike the model proposed by Stanway, Sproston, and Stevens (1987). It can be seen in Figure 2.6 which presents two force-velocity graphically. Part (a) shows the response of the Bingham Model and part (b) of the Modified Bingham Model. The black curves are the numerical values while the cyan curves represent values obtained experimentally. Despite the ability to represent the force-velocity behavior well, it is emphasized that the equations that govern the Modified Bingham Model are quite difficult to deal numerically, that being its main deficiency. The model is capable of representing well the MR damper force-displacement behaviors, as well as the Bingham model.

Figure 2.6 – Comparison of hysteresis between models proposed by Stanway *et al.* (1987) and Gamota, Filisko (1991)

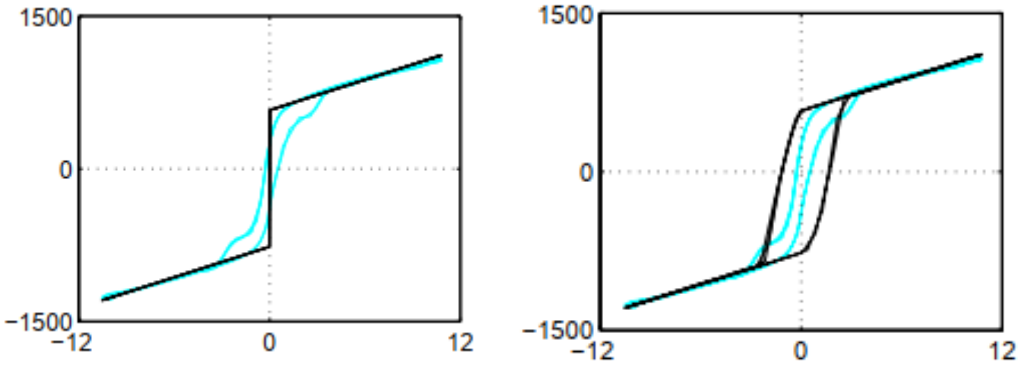

(a) Stanway *et al.* (1987) (b) Gamota, Filisko (1991)

Adapted from: Dyke (1996)

2.4 Bouc-Wen Model

The model proposed by Wen (1976) *apud* Dyke (1996) is numerically treatable and, for this reason, widely used. Figure 2.7 schematically represents this model which is called Bouc-Wen model. It is based on a Bouc-Wen element in parallel with a stiffness k and a viscous damping c.

Figure 2.7 – Bouc-Wen Model

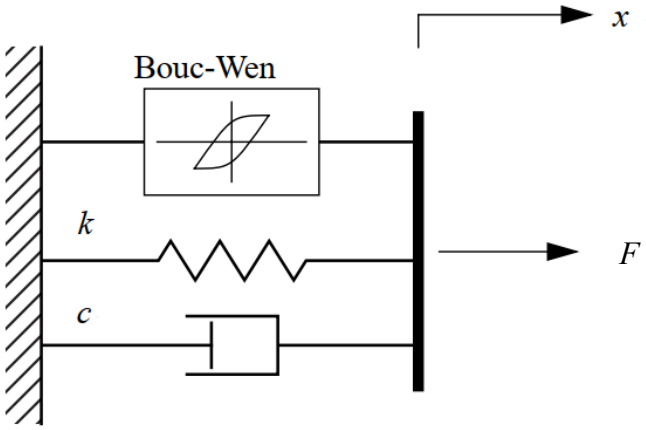

Source: Dyke (1996)

Damping force in the system is determined by Equation 2.5, where the parameters c, k, α, z e x_0 correspond to damping, stiffness, scale factor, evolutionary variable and initial displacement, respectively.

$$F = c\dot{x} + k(x - x_0) + \alpha z \tag{2.5}$$

The evolutionary variable z is obtained by Equation 2.6, updating the terms γ, β, δ, and n using some optimization method, and solving this differential equation. Such parameters depend on the characteristics of each damper and, through them, the smoothness of the transition in the inversion of the direction of speed and the linearities in the unloading are controlled. In addition, the residual force can be inserted in this model by means of an initial displacement x_0 in linear stiffness k, as described in Equation 2.5 (DYKE, 1996).

$$\dot{z} = -\gamma|\dot{x}|z|z|^{n-1} - \beta\dot{x}|z|^n + \delta\dot{x} \tag{2.6}$$

To adjust the cited parameters, Paschoal (2011) assumed the damping c, and the scale factor α as functions dependent on the electric voltage v applied to the actuator coil, proposing the relations provided in Equations 2.7, 2.8, and 2.9, where u is a resultant variable of a first order filter that represents the delay of the electric current in the circuit in relation to the input voltage. The factor η is also updated with the parameters presented on the right hand side of Equations 2.7 to 2.9.

$$\alpha(u) = \alpha_a + \alpha_b u \tag{2.7}$$

$$c(u) = c_a + c_b u \tag{2.8}$$

$$\dot{u} = \eta(u - v) \tag{2.9}$$

The Bouc-Wen model is able to accurately predict the MR damper force-displacement behavior and is able to more accurately approximate the force-velocity behavior obtained experimentally. This model was modified by some authors in search of obtaining a model capable of responding even closer to the experimental values, as will be presented below.

2.5 Modified Bouc-Wen Model

Dyke (1996) proposed a modification to the Bouc-Wen model, adding a viscous damping c_1 and a stiffness k_1 to the model, as shown in Figure 2.8. In this way, the author obtained a model capable of describing well the behavior of the MR damper in all regions, including the change in the direction of velocity.

Figure 2.8 – Modified Bouc-Wen Model

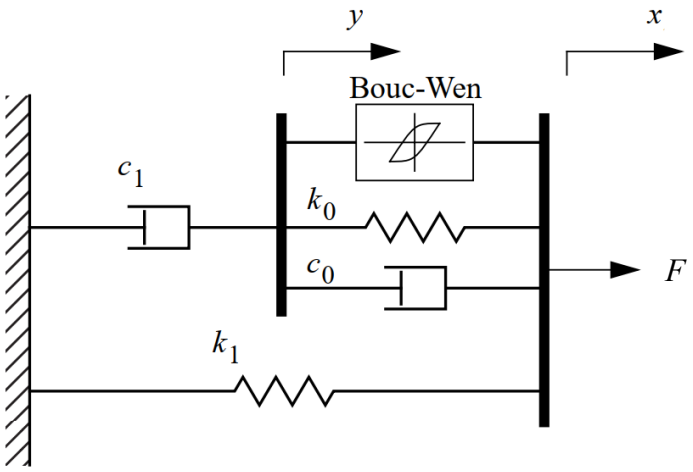

Source: Dyke (1996)

Damping force in the Modified Bouc-Wen Model is governed by Equations 2.10, 2.11 and 2.12. In these equations, the parameters c_0 and c_1 represent viscous damping, k_0 and k_1 linear stiffness, α is the scale factor, and z is the evolutionary variable. The parameters λ, β, and n depend on the physical characteristics of each damper, like the MR fluid used, brand and model of the damper, and the piston rest position, for example.

$$F = c_1\dot{y} + k_1(x - x_0) \tag{2.10}$$

$$\dot{y} = \frac{1}{c_0 + c_1}[\alpha z + c_0\dot{x} + k_0(x - y)] \tag{2.11}$$

$$\dot{z} = -\lambda|\dot{x} - \dot{y}||z|^{n-1} - \gamma(\dot{x} - \dot{y})|z|^n + \beta(\dot{x} - \dot{y}) \tag{2.12}$$

There are different ways to obtain the parameters of the Modified Bouc-Wen Model. The parameters can be adjusted as linear functions of the electric current, as did Teixeira (2017), by Equation 2.13 below, where i corresponds to the value of the applied electric current, and the values with indices a and b are obtained using optimization. Teixeira (2017) considers the parameters c_1 and k_1 independent of the electric current in the optimization.

$$\begin{aligned} c_0 &= c_{0a} \cdot i + c_{0b} & \alpha &= \alpha_a \cdot i + \alpha_b \\ k_0 &= k_{0a} \cdot i + k_{0b} & \beta &= \beta_a \cdot i + \beta_b \\ f_0 &= f_{0a} \cdot i + f_{0b} & \gamma &= \gamma_a \cdot i + \gamma_b \\ n &= n_a \cdot i + n_b & \lambda &= \lambda_a \cdot i + \lambda_b \\ c_1 &= c_1 & k_1 &= k_1 \end{aligned} \tag{2.13}$$

Another way of obtaining the parameters was proposed by Spencer *et al*. (1997). The values of the scale factor α and damping c_0 and c_1 were considered linear functions of the electric voltage, as described in Equations 2.14, 2.15, 2.16 and 2.17 below. Again, the variable u is the result of a first order filter that represents the delay of the electric current in the circuit in relation to the input electric voltage.

$$\alpha(u) = \alpha_a + \alpha_b u \tag{2.14}$$

$$c_0(u) = c_{0a} + c_{0b} u \tag{2.15}$$

$$c_1(u) = c_{1a} + c_{1b} u \tag{2.16}$$

$$\dot{u} = \eta(u - v) \tag{2.17}$$

Such an approach is known in the literature as the Phenomenological Model, and has the advantage of reducing the number of parameters to be adjusted. Because it responds well to hysteresis behavior, this modeling was adopted by Paschoal (2011) and Cavalini Júnior *et al*. (2015).

2.6 Hysteretic Model

The Hysteretic Model proposed by Kwok *et al*. (2006) models the transient effect of the actuator well. Teixeira (2017) compared several parametric models and obtained the hysteresis curve closest to the experimental data using this model.

Figure 2.9 – Hysteretic Model

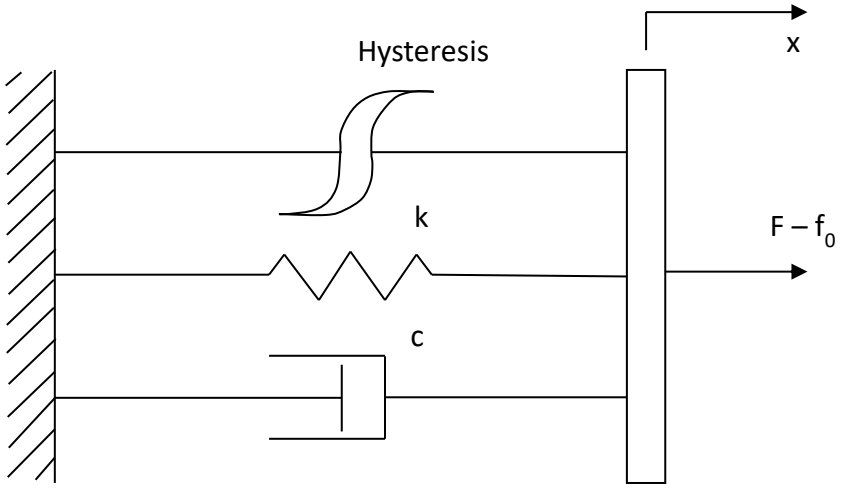

Adapted from: Kwok (2006)

Such model, like the Bouc-Wen model, consists of viscous damping parallel to linear stiffness and an element related to hysteresis, as shown in Figure 2.9. However, the hysteretic variable z is modeled only as a hyperbolic tangent, as can be seen in Equation 2.19, which makes the model quite simple to implement numerically (KWOK, 2006).

$$F = c\dot{x} + kx + \alpha z + f_0 \tag{2.18}$$

$$z = \tanh\left(\beta\dot{x} + \delta sign(x)\right) \tag{2.19}$$

The damping force is described in Equation 2.18, where c and k are damping and stiffness, respectively. α is the scale factor, z is the hysteretic variable, and f_0 is the residual force. The constants β and δ in Equation 2.19 are parameters to be adjusted according to the electric current, as shown in Equation 2.20.

$$\begin{aligned} c &= c_a \cdot i + c_b \\ k &= k_a \cdot i + k_b \\ \alpha &= \alpha_a \cdot i^2 + \alpha_b \cdot i + \alpha_c \\ f_0 &= f_{0a} \cdot i + f_{0b} \\ \beta &= \beta \\ \delta &= \delta_a \cdot i + \delta_b \end{aligned} \tag{2.20}$$

CHAPTER III

FUZZY SETS

"There is nothing worse than a sharp image of a fuzzy concept."
– Ansel Adams

3.1 Introduction

As mentioned in Chapter 1, fuzzy logic emerged by the need to represent systematically imprecise quantities. This need derives from the fact that not all systems require or are capable of inputting and outputting accurate values.

Fuzzy, as a mathematical concept, was first called that way by Zadeh (1965) in his work entitled 'Fuzzy sets'. According to Pelletier (2000), the same theory was previously investigated since the 1920's by authors like Lukasiewicz and Tarski under the name of 'infinite-value logic'. Mamdani (1974) sized up applications of fuzzy logic in the synthesis of controllers for dynamic plants, Takagi; Sugeno (1985) presented a mathematical tool to build fuzzy models, and many other authors helped to develop studies in this field.

The great difference between fuzzy logic and traditional Boolean algebra is the act of attributing pertinence degrees (the 'significance') to membership functions (MF), instead of precise values to variables. Such concept can be applied widely, from the financial to the medical sectors, passing through refrigerator and camera technology, fuzzy logic theory led to many advances and it is object of study by many researchers since its conception. Fuzzy logic controllers, for example, decreased the development time and the deployment cost for nonlinear controllers for dynamic systems. The applications can be seen in turboshaft aircraft engine control, steam turbine startup, and steam turbine cycling optimization (BONISSONE *et al*, 1995). Thus, there are several applications of fuzzy theory on renewable energy systems. Sughanti, Iniyan, and Samuel (2015) summarized some of these applications, like using fuzzy

to manage energy systems under multiple uncertainties to identify optimal strategies in that context.

In mechanical engineering, fuzzy sets can be used to analyze inputs and outputs of mechanical systems. The deformation of a mechanical part, for example, depends on several factors. The engineer uses some criteria to determine which premises are significant to the system and then understands the process. By selecting temperature and stress as inputs to analyze strain, it can be observed that higher temperatures increase the deformation with moderate loads.

Originally, the rules of a fuzzy inference system (FIS) were set by the domain expert knowledge. With the aim of controlling nonlinear systems without the dependence of expertise about the plant, Jang (1992) developed a self-learning mechanism able of derive the membership functions of the rules used by fuzzy systems based on adaptative networks. Such a method expanded the range of applications of fuzzy controllers and their implementation feasibility.

3.2 Fundamentals

The definitions made by Zadeh (1965) were explained by Jafelice (2003). Both works serve as basis for the following definitions and their reading is suggested for a deeper understanding of fuzzy theory.

A fuzzy set A in a universe X is characterized by a membership function $f_A(x)$ which is related to a significance parameter: the 'grade of membership', as called by Zadeh (1965). Such a parameter is a real number in the interval [0, 1]. When zero is attributed means x has no pertinence in A, and the closer the value is to the unity the higher the pertinence of x in A. Two fuzzy sets A and B are equal if and only if $f_A(x) = f_B(x)$ for all x in X.

Let A and B be fuzzy sets in the universe X. The sets

$$A \cup B = \{x \in X \mid x \in A \; or \; x \in B\} \tag{3.1}$$

$$A \cap B = \{x \in X \mid x \in A \; and \; x \in B\} \tag{3.2}$$

$$A' = \{x \in X \mid x \notin B\} \tag{3.3}$$

have the following characteristic functions

$$f_{A \cup B}(x) = \max\{ f_A(x), f_B(x) \}, \forall x \in X \tag{3.4}$$

$$f_{A\cap B}(x) = \min\{ f_A(x),\ f_B(x)\ \}, \forall x \in X \tag{3.5}$$

$$f_{A'}(x) = 1 - f_A(x), \forall x \in X \tag{3.6}$$

where Equation 3.4 represents the grade of membership of the union set, Equation 3.5 represents the grade of membership of the intersection set, and Equation 3.6 represents the grade of membership of the complement set for fuzzy operations. Both union and intersection have the associative property, that is, $A \cup (B \cup C) = (A \cup B) \cup C$ and $A \cap (B \cap C) = (A \cap B) \cap C$. Algebraic operations like sum and product are also possible on fuzzy sets.

According to Zadeh (1965), the algebraic sum of *A* and *B* is denoted by $A + B$ and is defined in terms of the membership function by $f_{A+B} = f_A + f_B$. Similarly, the algebraic product of *A* and *B* is denoted by *AB* and is defined in terms of the membership function by $f_{AB} = f_A f_B$.

Cartesian product of fuzzy sets is important for fuzzy rule-based systems. The general definition of a cartesian product $R(x_1, x_2, \dots, x_n)$ of the fuzzy sets $A_1, A_2, \dots, A_n$ in the domain $X_1, X_2, \dots, X_n$ is the fuzzy relation

$$R(x_1, x_2, \dots, x_n) = A_1(x_1) \wedge A_2(x_2) \wedge \dots \wedge A_n(x_n) \tag{3.7}$$

where $\wedge$ is the t-norm operator Jafelice (2003). T-norm is also known as s-conorm and can be defined as

$$T[f_A(x), f_B(x)] = f_{A\cap B}(x), \forall x \in X \tag{3.8}$$

Inputs and outputs of fuzzy systems are related to each other by fuzzy rules. These rules are ‘if-then’ premises that make possible to infer the output depending on input values. The relations make use of linguistic variables. For example, ‘IF displacement IS large THEN action’ governs a generic control output, with variables ‘displacement’, ‘action’ and ‘large’. The full set of linguistic variables in such example could be, for displacement, $D = \{small,\ medium,\ large\}$ and, for output, $O = \{action,\ no\ action\}$. The relations (operations) between linguistic variables are carried out under the definition of cartesian products presented in Equation 3.7. A practical example presented in the next topic will make it clearer.

3.3 Fuzzy Rule-Based Systems (FRBS)

Jafelice (2003) described FRBSs in four components: an input processor (fuzzification), a set of fuzzy rules, an inference machine and an output processor (defuzzification). Fuzzy Rule-Based Systems are also known as Fuzzy Inference Systems (FIS). The architecture of this type of system is shown in Figure 3.1.

Figure 3.1 – Fuzzy Rule-Based System Architecture

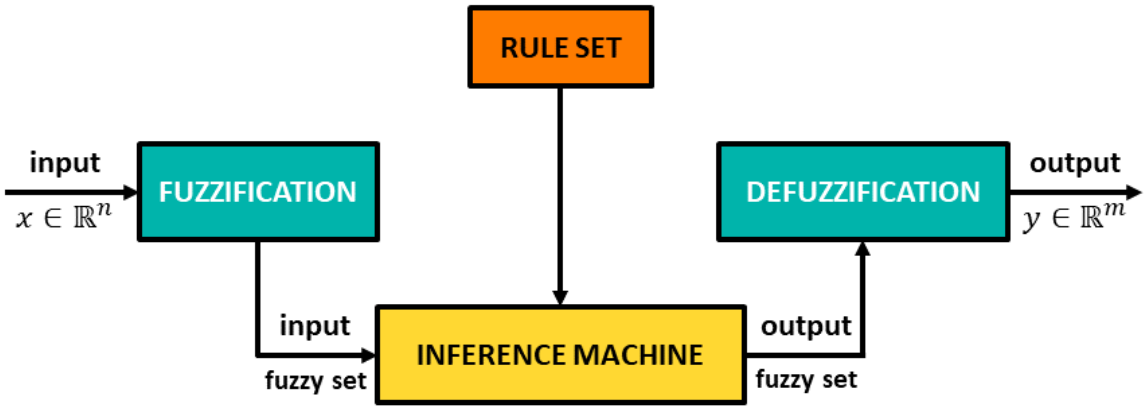

Adapted from: Jafelice (2003)

The input processor, represented by the 'fuzzification' box, converts real numbers in fuzzy sets, that is, acts as a fuzzification interface transforming crisp quantities in fuzzy quantities. These quantities will be subjected to operations in the inference machine together with fuzzy rules. A specialist is required in this step to model the number membership functions and the grade of membership of each input parameter to the respective domain. Membership functions can be modeled in numerous shapes. The most common are triangular, gaussian and trapezoidal shapes.

The box named 'rule set' contains the basis of fuzzy 'if-then' rules to be used in the inference machine. All relations between linguistic variables are described in this step, and can be modeled according to the specialist's knowledge. This component, together with the inference machine, can be considered the kernel of fuzzy rule-based systems.

Outputs from the fuzzification interface are inputs for the inference machine together with the fuzzy rules. It acts as a decision-making unit, performing operations on rules and each proposition using approximation techniques. The two most used methods available to this end are Mamdani Method and Takagi-Sugeno Method. Some details of each method are presented in the following subtopics.

3.3.1 Mamdani Method

This method relates each 'if-then' rule via an 'or' operator or an 'and' operator. Equations 3.1 and 3.4 showed that 'or' is a maximum operator and Equations 3.2 and 3.5 showed that 'and' is a minimum operator for operations with fuzzy sets. It can be understood by the following example. Set two fuzzy rules: Rule 1: IF (x is A_1 and y is B_1) THEN (z is C_1). Rule 2: IF (x is A_2 and y is B_2) THEN (z is C_2). The inference machine output computes the cartesian product of the antecedent sets (*if*) and the consequent sets (*then*). The antecedent proposition of Rules 1 and 2 use the operator 'and'. Then, the minimum between the grade of membership of x in $A_1 \in X$ and y in $B_1 \in Y$ will be evaluated based on Rule 1, and the grade of membership of x in $A_2 \in X$ and y in $B_2 \in Y$ will be evaluated based on Rule 2. The union of these fuzzy sets generates the output $C = C_1' \cup C_2'$ to be deffuzificated by the output processor, as Figure 3.2 illustrates.

Figure 3.2 – Mamdani Method

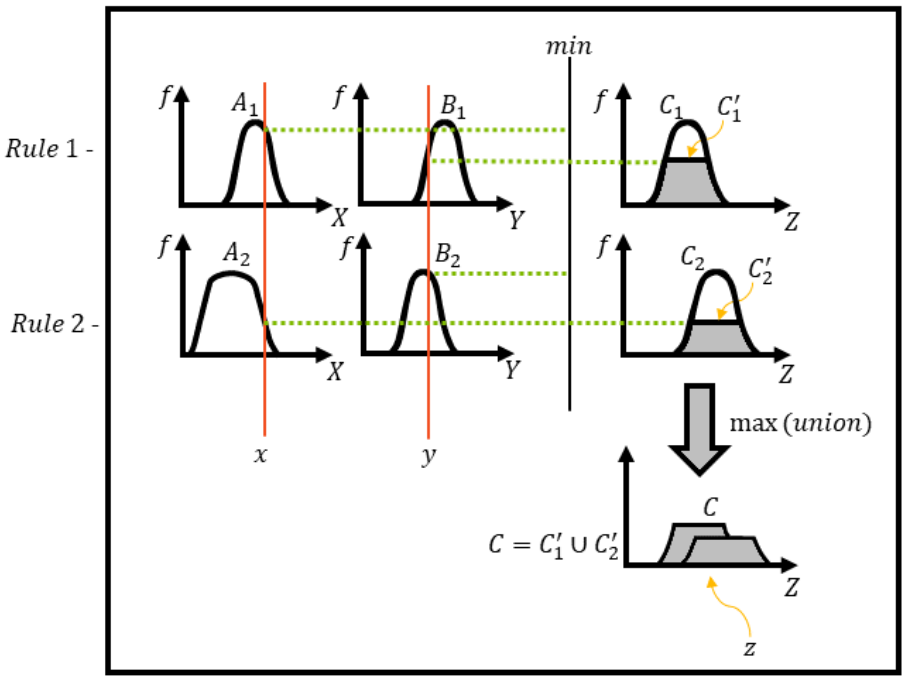

Adapted from: Jafelice (2003)

3.3.2 Takagi-Sugeno Method

This method's consequent (*then*) is a function of input variables. That is, a linear combination of inputs is used to represent input relations for each rule on the form $z_i = p_i x + q_i y + r_i$. Considering two fuzzy rules: Rule 1: IF (x is A_1 and y is B_1) THEN [$z_1 = f_1(x, y)$].

Rule 2: IF (x is A_2 and y is B_2) THEN [$z_2 = f_2(x, y)$]. Figure 3.3 illustrates how the inference machine generates the output z using this method.

Figure 3.3 – Takagi-Sugeno Method

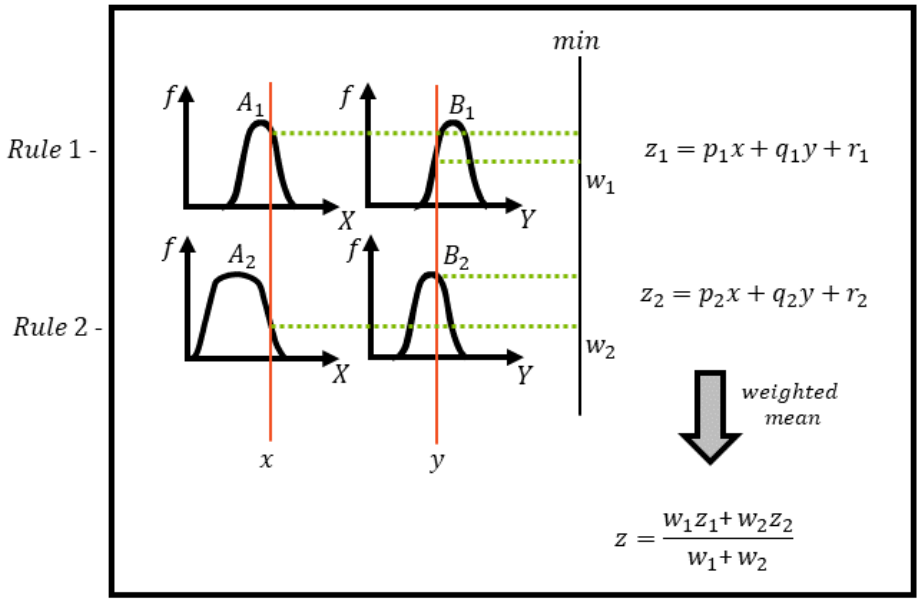

Adapted from: Jafelice (2003)

Similar to Mamdani, the minimum between the grade of membership of x in $A_1 \in X$ and y in $B_1 \in Y$ will be evaluated based on Rule 1, and the grade of membership of x in $A_2 \in X$ and y in $B_2 \in Y$ will be evaluated based on Rule 2. But, instead of a union set, the cartesian products are considered as weights (w_1 and w_2) for the weighted mean (deffuzification) calculated together with the linear combinations of inputs (z_1 and z_2). Such combinations depend on the system's characteristics. For example, Rule 1: "IF displacement is *low* and damping is *low* THEN force is $F = m\ddot{x} + kx$; Rule 2: "IF displacement is *low* and damping is *high* THEN force is $F = m\ddot{x} + c\dot{x} + kx$. Note that, in this playful case, $\ddot{x}$, $\dot{x}$ and x are input values (real numbers) and not variables.

3.3.3 Defuzzification

Similar to fuzzification, the defuzzification interface does the opposite, converting fuzzy quantities into crisp values in the domain of real numbers. As shown in Figure 3.3, the weighted mean is the deffuzification method used in systems based on Takagi-Sugeno Method. The output z is obtained generically by solving Equation 3.9.

$$z = \frac{\sum_{i=1}^{k} w_i z_i}{\sum_{i=1}^{k} z_i} \tag{3.9}$$

where i is the i-th rule and k is the number of fuzzy rules.

Another deffuzification method, the most common, according to Jafelice (2003), is the centroid method, expressed in Equations 3.10 and 3.11 for discrete and continuous domain, respectively. z_i is the i-th output from the inference machine and k is the number of fuzzy rules.

$$\bar{z} = \frac{\sum_{i=1}^{k} f_i(z_i) \cdot z_i}{\sum_{i=1}^{k} z_i} \tag{3.10}$$

$$\bar{z} = \frac{\int_R f_i(z) \cdot z \cdot dz}{\int_R z \cdot dz} \tag{3.11}$$

Such a method resembles the weighted mean. The difference is that the weights are $f_i(z_i)$ values that represent the grade of membership of z_i to f_i. It can be seen in Figure 3.4, where R is the yellow area and stands for the integration region. The green curve represents fuzzy set A and curve red represents fuzzy set B. Depending on the operation between A and B (*and* or *or*), a different R will be obtained. Centroid values of $A \cap B$ and $A \cup B$ are not necessarily equal.

Figure 3.4 – Representation of union and intersection of fuzzy sets

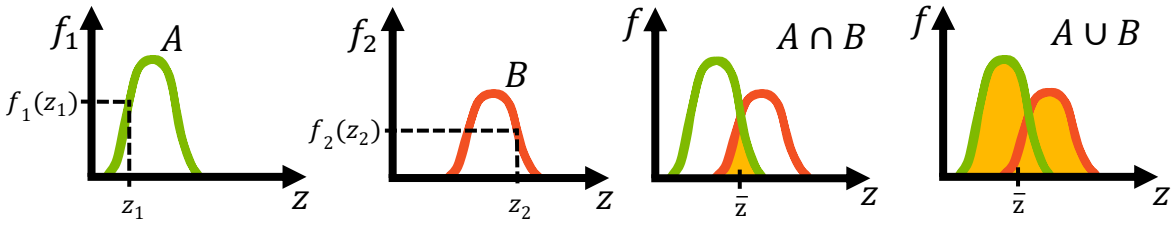

Source: Elaborated by the author

3.4 Adaptive Neuro-Fuzzy Inference Systems (ANFIS)

The dependence on an expert to model the membership functions and their characteristics motivated researchers to seek alternatives for such modeling. Jang (1992) combined Adaptive Neural Networks (ANN) with FRBS structure giving rise to Adaptive Neuro-Fuzzy Inference Systems (ANFIS). Neural networks are a type of mathematical model that has some internal coefficients (weights and bias). During training, input and output values

are assigned to the network inputs and outputs, aiming to minimize the network's output error compared to the desired output data.

Nedjah; Mourelle (2005) does a deep dive on the theory behind ANFIS modeling. For this work purposes, the focus is on adaptive neuro-fuzzy systems that use Takagi-Sugeno Method. These systems normally use backpropagation to learn the membership functions and least mean square estimations to determine the coefficients of the linear combinations in the rules's conclusions. However, some works use different optimization techniques, as Chen; Lin; Lin (2009), Pereira (2017) and Sant'ana (2019) used Differential Evolution to tune their neuro-fuzzy systems.

Figure 3.5 – Takagi-Sugeno ANFIS architecture

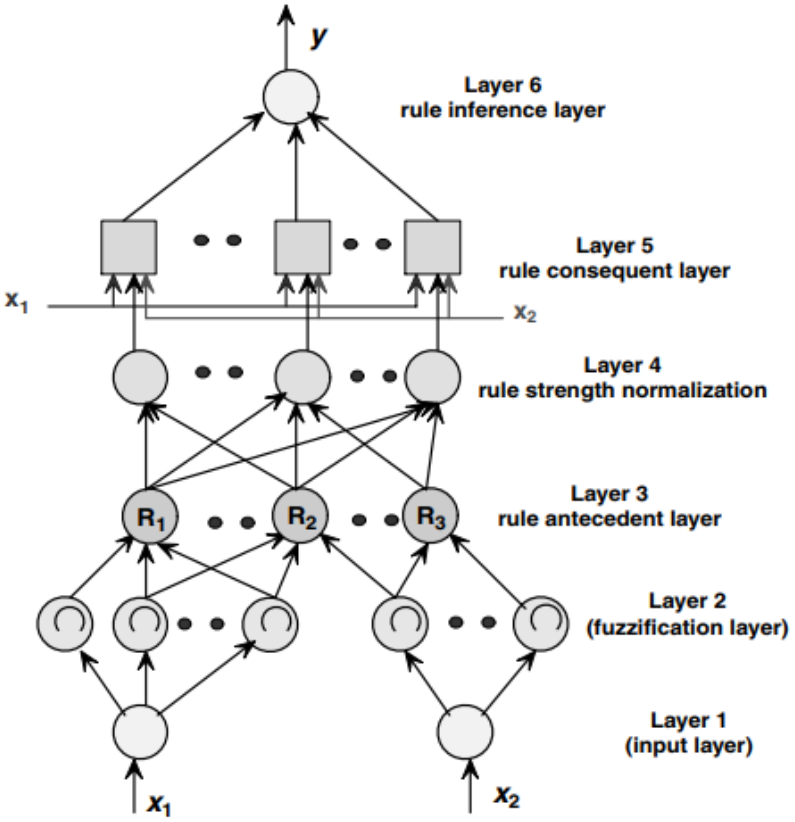

Source: Nedjah; Mourelle (2005)

Figure 3.5 shows the structure of a Takagi-Sugeno ANFIS. Each node of Layer 1 (*input layer*) receives an input (x_1 and x_2) and passes it directly to the next layer. No mathematical operation is done in this step.

Fuzzification is done in Layer 2 (*fuzzification layer*). After building the membership functions (MF), what is done by a clustering algorithm that decides the initial number of

membership functions and their type with respect with each input variable, the grade of membership is calculated. Each node of this layer represents a linguistic variable, as *high* or *low* for example.

Each node of Layer 3 (*rule antecedent layer*) corresponds to the antecedent part of a rule, i.e., a fuzzy quantity to be computed, commonly by a triangular norm (t-norm), with the consequent part. The output of the nodes in layer 3 is, as called by Nedjah; Mourelle (2005), the 'firing strength' of the corresponding fuzzy rule.

In Layer 4 (*rule strength normalization*), a ratio between the i-th rule's firing strength and the sum of all rules' firing strength is calculated in each node, as show Equation 3.12. This gives normalized weights for each node output.

$$\overline{w}_i = \frac{w_i}{w_1 + w_2}, i = 1, 2 \ldots \tag{3.12}$$

Each node on Layer 5 (*rule consequent layer*) has a node function in the form described in Equation 3.13, where $\overline{w}_i$ is the output from layer 4 and the parameters p_i, q_i and r_i are coefficients of inputs, as exposed in the previous topic. These coefficients are usually determined by using least mean squares algorithm.

$$\overline{w}_i f_i = \overline{w}(p_i x_1 + q_i x_2 + r_i) \tag{3.13}$$

Layer 6 (*rule inference layer*) sums all signals from layer 4 as an overall output described in Equation 3.14.

$$Overall\ output = \sum \overline{w}_i\, f_i = \frac{\sum w_i f_i}{\sum \mathrm{w}_i} \tag{3.14}$$

To obtain the ANFIS weights, the system must be trained using some optimization method to tune the model's internal coefficient minimizing the error between the model output and the desired output. The next three subtopics are dedicated to give an overview of three optimization methods relevant to this work: backpropagation, least squares and differential evolution.

3.4.1 Backpropagation

Nielsen (2015) explain in details how the backpropagation algorithm works. The following concepts are based on his book entitled "Neural networks and deep learning". Backpropagation's main goal is to compute a gradient of a cost function C with respect to weights w and bias b of a neural network ($\partial C/\partial w$ and $\partial C/\partial b$) to have a measure of how changes in weights and biases affect C. To this end, an error function δ_{lj} is introduced in the *j-th* neuron in the *l-th* layer as an intermediate quantity. Then, backpropagation provides a procedure to compute such error and relate it to the gradient.

In synthesis, the algorithm starts by receiving an input activation for the input layer. Then, a feedforward step is done by computing activations as functions of weights and bias. A vector of error is provided and propagated on each layer backwards (the reason why the algorithm is called backpropagation). Finally, the gradient of cost function is obtained.

3.4.2 Least Squares

One of the most used approximation techniques in numerical analysis and practical problems is the Least Squares Method. This is due both to its simplicity and to the fact that, in general, authors seek approximations for experimentally obtained data with a certain degree of uncertainty. The approximation strategy is to minimize the residual distance r_i between each point in the database y_i and its respective point in a curve, Equation 3.15, obtained by the method as a function f of data x_i and parameters α as shows Equation 3.16. The subscript i stands for the *i-th* value from database and n is the number of individuals to be fit (RUGGIERO; LOPES, 1997).

$$f(x, \alpha_i) = \alpha_1 + \alpha_2 x + \alpha_3 x^2 + \cdots + \alpha_{n+1} x^n \tag{3.15}$$

$$r_i = y_i - f(x_i, \alpha) \tag{3.16}$$

The least squares method finds an optimal value of the parameter vector by minimizing the sum of squared residuals S as expressed in Equation 3.17.

$$S = \sum_{i=1}^{n} r_i^2 = \sum_{i=1}^{n} [y_i - f(x_i, \alpha)]^2 \tag{3.17}$$

3.4.3 *Differential Evolution*

Differential Evolution (DE) is an evolutionary algorithm that has the advantage of achieving global minimums of non-linear or non-differentiable continuous space functions faster and more accurate when compared to other heuristic methods. This algorithm requires few variables what makes it easy to deal and implement (STORN; PRICE, 1996). Figure 3.6 shows a representation of DE. According to Pereira (2017), it is divided in four steps: initialization, mutation, crossover, and selection.

Figure 3.6 – Differential evolution schematic

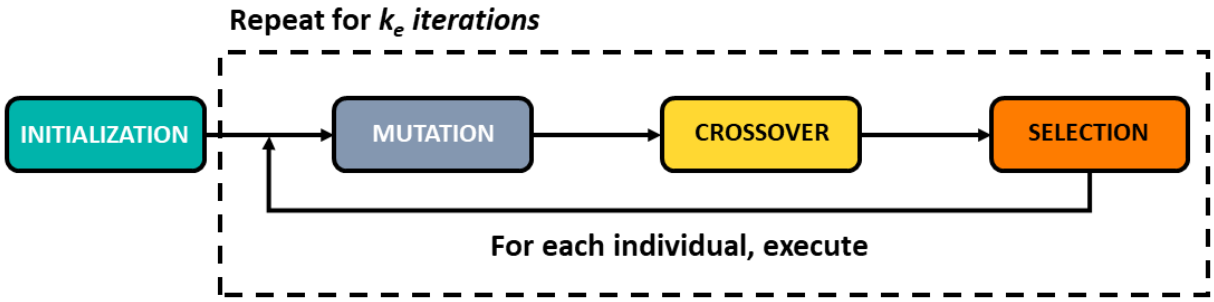

Adapted from: Mór *et al* (2015) *apud* Pereira (2017)

At the initialization, the parameter values used throughout the iterations and the stop criteria for each variable are defined, i.e., each $X_{i,0}$ that contains a possible solution for the fitness function is initialized and their fitness to the objective function (f_{obj}) is calculated. Then, the mutation changes the values of $X_{i,k}$ as expressed in Equation 3.18, where $V_{i,k}$ is the vector obtained at iteration k from $X_{i,k}$, $X_{j,k}$, and $X_{l,k}$ are random vectors from population set at iteration k, and F is the perturbation factor for the vector $X_{i,k}$.

$$V_{i,k} = X_{i,k} + F\left(X_{j,k} - X_{l,k}\right) \tag{3.18}$$

$$C_{e,i,k} = \begin{cases} V_{e,i,k}, IF\ rand(0,1) \leq CR\ OR\ e = randnum(1, n_e) \\ X_{e,i,k}, IF\ rand(0,1) > CR\ AND\ e \neq randnum(1, n_e) \end{cases} \tag{3.19}$$

A recombination is done at the crossover stage. It aims to mix data present in vectors $V_{i,k}$ and $X_{i,k}$ to guarantee diversity in the population. For each element e from vector $V_{i,k}$, a value between zero and one is generated by $rand(0,1)$ and compared to a crossing rate CR. Equation 3.19 specifies the decision making for this recombination process, where $C_{i,k}$ is the candidate solution on for the next iteration and n_e is the number of vector elements.

Selection is the last DE operator. It analyses the $C_{i,k}$ generated at the recombination. Equation 3.20 shows the selection criteria to be done for all vectors in solution set. After selection, the next iteration starts, and the steps are repeated until the stop criteria is achieved.

$$X_{i,k+1} = \begin{cases} X_{i,k}, if\ f_{obj}(X_{i,k}) \leq f_{obj}(C_{i,k}) \\ C_{i,k}, if\ f_{obj}(X_{i,k}) > f_{obj}(C_{i,k}) \end{cases} \tag{3.20}$$

That said, differential evolution was used on the parameter fitting process for the parametric models. Backpropagation and least squares were used for the ANFIS with Takagi-Sugeno inference method. The details are presented in the next chapter.

CHAPTER IV

COMPARISON OF MR DAMPER MODELS

"It doesn't matter how beautiful your theory is, it doesn't matter how smart you are. If it doesn't agree with experiment, it's wrong."

– Richard P. Feynman

4.1 Introduction

There is a trend in literature for authors to seek mathematical expressions capable of modeling magnetorheological dampers more efficiently. Teixeira (2017), in his master's dissertation, brought a comparison between the parametric models mentioned in Chapter 2 of this work and a non-parametric model, using fuzzy logic. To this end, an experiment was carried out to characterize an MR actuator of the LORD brand and model RD-8040-1 at the LMEst of Federal University of Uberlandia (UFU). All the experimental values considered in the present work are results of such experiment.

4.2 Experimental Overview

Teixeira (2017), used a servo-hydraulic MTS Landmark® machine, model 370.10, to characterize the MR damper. The idea of this type of test was to subject the damper to a sinusoidal displacement previously configured. In other words, the damper stroke was moved at a defined frequency and displacement. Then, the force expended for such movement was observed. The force data is the force applied by the machine on the MR damper, whose values correspond to the damping force. The obtained results are presented in Figure 4.1, and the assembly of the test is shown in Figure 2.

Figure 4.1 – MR damper characterization

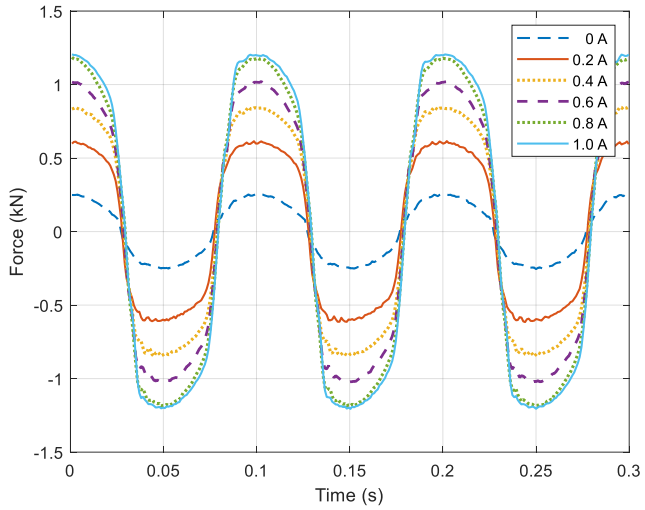

(a)

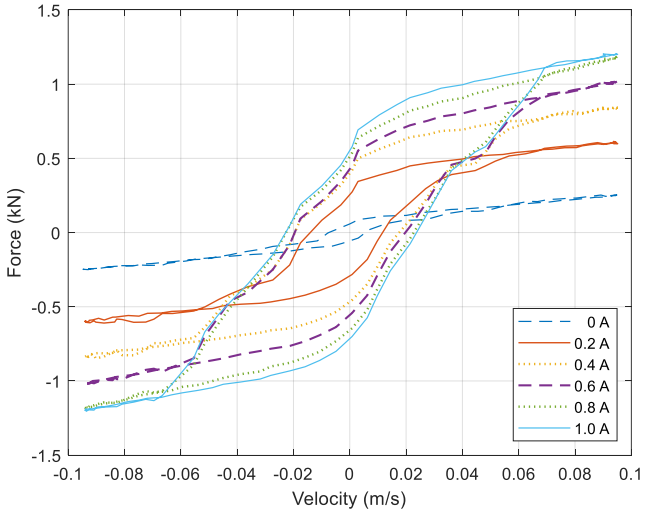

(b)

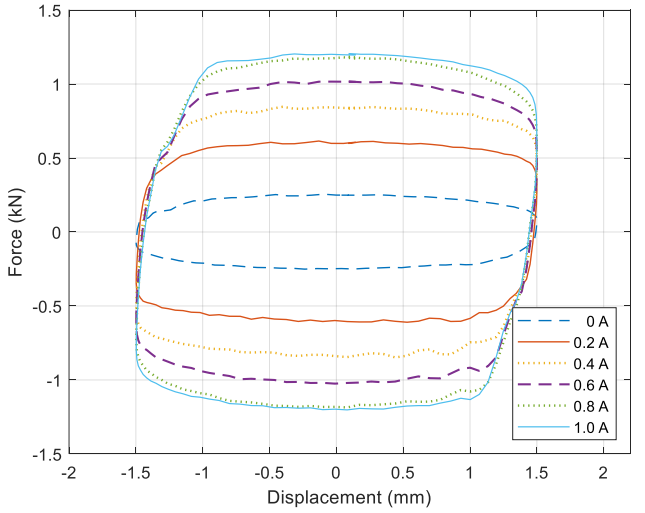

(c)

Source: Elaborated by the author

The electric current is also an input parameter for this type of test and is a linear function of electric voltage. As can be seen in Figure 4.1, the damping force increases according to the electric current as resistance to motion generated by the MR damper. When subjected to a magnetic field it increases. However, a saturation region is observed. From a certain point onwards, the increase in the intensity of the electric current does not imply a proportional increase in the damping force. That happens because the MR fluid's magnetic particles are fully aligned to the magnetic field and can't align themselves more than they already are.

Figure 4.2 – Experimental gear

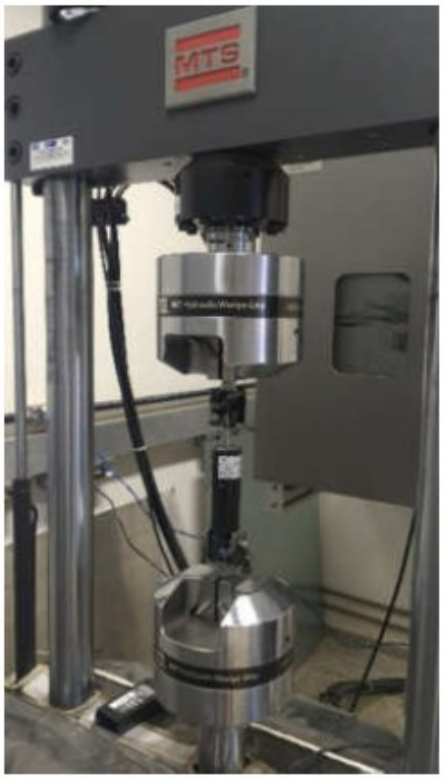

Source: Teixeira (2017)

The results presented in Figure 4.1 were obtained for a frequency of 10 Hz, amplitude displacement of 3 mm, and electric current ranging from 0 A to 1.0 A, increasing in steps of 0.2 A. Figure 4.1a represents the dynamic response of the damping force over time. Figure 4.1b shows the hysteresis curve, in which a greater energy dissipation is observed to perform the same displacement in the actuator, as the electric current increases. Similarly, Figure 4.1c illustrates the relation between force and displacement obtained, in which the machine increases the intensity of the force necessary to promote the same displacement, also according to the electric current.

4.3 Parametric Models

In this section, a study of Modified Bouc-Wen and Hysteretic model is performed. The uptading of parameters associated with each model was performed using optimization with Differential Evolution algorithm proposed by Storn and Price (1997). The objective function aims to minimize the deviation (error) between force values obtained numerically and experimentally. That is, the minimum of the quotient between the norm of the difference of the numerical and experimental values of force and the norm of the experimental values of force, as given by Equation 3.1.

$$f_{\text{obj}} = minimize\left[\frac{\left\|\mathrm{F}_{\text{numerical}} - \mathrm{F}_{\text{experimental}}\right\|}{\left\|\mathrm{F}_{\text{experimental}}\right\|}\right] \tag{4.1}$$

Four scenarios of simulation, shown in Table 4.1, were performed to analyze the parametric models. In scenario *A*, the parameters were updated for each value of electric current and solved for the same value of electric current that the parameter fitting was done. This is expected to be the closest the model can get to experimental values. In scenario *B*, all the optimized models in scenario *A* are solved for the same electric current value (0.6 A) and overlapped. In an ideal situation, the results calculated for each model should be the same. Note that each parameter fitting represents one model with different parameters and that was done for both Modified Bouc-Wen and Hysteretic models, as explained before. In scenario *C*, the parameters obtained for 0.6 A in scenario *A* are solved for each electric current analyzed. Then, in scenario *D*, the same is done for the parameters obtained for 1.0 A in scenario *A*. The purpose of this is to observe the impact of the selected value of electric current for the optimization in the accuracy of the model.

Table 4.1 – Scenarios of Simulation

Scenario	Description
A	six different models solved for six different values of electric current
B	six different models solved for the same value of electric current
C	model adjusted for 0.6 A solved for six different values of electric current
D	model adjusted for 1.0 A solved for six different values of electric current

Source: Elaborated by the author

4.3.1 Modified Bouc-Wen Model

The obtained parameters for the Modified Bouc-Wen model are presented in Table 4.2. In the optimization, it was considered a maximum of 200 generations for the 18 variables, a population size of 360 individuals, and 0.8 for mutation, and crossover probability. The range of search used to update each parameter is shown in Table 4.3 with their respectives lower and upper bounds.

Table 4.2 – Parameters for modified Bouc-Wen model

	0 A	**0.2 A**	**0.4 A**	**0.6 A**	**0.8 A**	**1.0 A**
c_{0a}	3178.27	2001.24	2091.29	2842.23	3881.18	3075.68
c_{0b}	4500.01	4500.00	4513.19	5336.02	5122.17	4514.26
k_{0a}	7000.00	6115.13	7000.00	6609.54	7000.00	6711.34
k_{0b}	9273.62	14028.67	12994.59	30000.00	29969.10	29937.62
α_a	788.21	894.49	855.22	715.38	581.13	520.93
α_b	300.29	518.10	478.26	337.99	315.20	300.00
f_{0a}	552.71	293.02	556.88	600.00	491.78	200.00
f_{0b}	152.13	247.29	250.00	80.00	217.39	131.89
n_a	1.71	2.10	3.48	3.50	3.49	3.50
n_b	1.00	3.53	4.00	4.00	3.99	4.00
γ_a	134000.70	135831.05	90776.97	80000.00	80105.91	82167.09
γ_b	350000.00	333239.49	100000.00	101171.07	100519.84	100000.00
λ_a	8000.00	8000.00	8031.41	8021.91	8008.42	8025.55
λ_b	10015.24	10607.79	10000.00	10002.25	10001.61	10005.90
β_a	-600000.00	-497206.08	-596085.91	-567784.27	-600000.00	-600000.00
β_b	3000000.00	1000000.00	1004078.35	1000000.00	1000000.00	1000000.00
c_1	600000.00	600000.00	636136.36	766198.09	741164.57	800000.00
k_1	10000.00	14068.80	40073.32	48977.11	50000.00	49758.10

Source: Elaborated by the author

Table 4.3 – Search Space for the optimized parameters in Modified Bouc-Wen Model

Parameter	c_{0a}	k_{0a}	α_a	f_{0a}	n_a	γ_a	λ_a	β_a	c_1
lower	2000	4000	500	200	1.0	80000	8000	-600000	600000
upper	4000	7000	2000	600	3.5	200000	20000	-400000	800000
Parameter	c_{0b}	k_{0b}	α_b	f_{0b}	n_b	γ_b	λ_b	β_b	k_1
lower	4500	9000	300	80	1.0	100000	10000	1000000	10000
upper	7000	30000	600	250	4.0	350000	35000	3000000	50000

Source: Elaborated by the author

Table 4.4 shows the calculated errors for all simulation scenarios. These values were obtained using Equation 4.2, which is the same argument used in Equation 4.1. It is observed that for zero electric current, error values are higher. It is a consequence of the architecture used to fit the parameters which consisted in functions of electric current, as presented in Equation 2.13. For $i = 0$, some parameters are negleted and the model becomes less representative.

$$\text{error} = \frac{\left\| \text{F}_{\text{numerical}} - \text{F}_{\text{experimental}} \right\|}{\left\| \text{F}_{\text{experimental}} \right\|} \tag{4.2}$$

Considering the range of electric current analyzed, the smallest errors in scenarios *A* and *B* are closest to the middle, *i.e.*, far from the saturation region and the region of zero electric current. It happens due to the model's weakness in representing the nonlinearities intrinsic on MR fluids and its lost in mathematical representation for small values of electric current.

Table 4.4 – Errors compared to experiment for Modified Bouc-Wen Model

	0 A	**0.2 A**	**0.4 A**	**0.6 A**	**0.8 A**	**1.0 A**
error^A	56.09 %	10.34 %	8.23 %	8.71 %	9.59 %	11.22 %
error^B	46.60 %	13.09 %	9.96 %	8.71 %	9.29 %	16.44 %
error^C	138.24 %	21.02 %	10.18 %	8.71 %	10.42 %	20.26 %
error^D	107.49 %	18.79 %	17.92 %	16.44 %	15.01 %	11.22 %

Source: Elaborated by the author

Figure 4.4 shows the obtained results for the simulations of scenarios *A* and *B*. The indexes *a* and *b* are related to time versus damping force, *c* and *d* to velocity versus damping force and *e* and *f* to displacement versus damping force. In scenario *B* the data is not perfectly overlapped. This is another indicative that the selected value of electric current for the parameter fitting impacts the model's ability to represent the experiment.

Figure 4.5 shows the obtained results for the simulations of scenarios *C* and *D*. The indexes are analog to Figure 4.4. The impact observed in scenario *B* is quantified in scenarios *C* (parameters updating to 0.6 A) and *D* (parameters updating to 1.0 A). The closer to the selected electric current for optimization, the smallest are the errors. That can be observed in Figure 4.3, where errors from scenarios *C* and *D* are shown.

In scenario *C*, the model predicts reasonably well the damping force behavior for 0.4 A and 0,8 A with deviations of 10.18 % and 10.42 %, respectively, which are similar values to 8.71 % that corresponds to 0.6 A. However, the deviations aproximately double on the next step of electric current, with 21.02 % for 0.2 A and 20.26 % for 1.0 A. The same is observed in scenario *D* which error values are smaller next to 1.0 A and increase as values are calculated further away from it. Furthermore, the standard deviation of errors in scenario *C* and *D* are 51.0 % and 37.5 %, respectively. That indicates that fitting the parameters close to saturation region gives more precision for Modified Bouc-Wen model. Mean values of errors are similar: 34.8 % and 31.1 % for *C* and *D*, respectively.

Figure 4.3 – Comparison of errors between scenarios *C* and *D* (Modified Bouc-Wen)

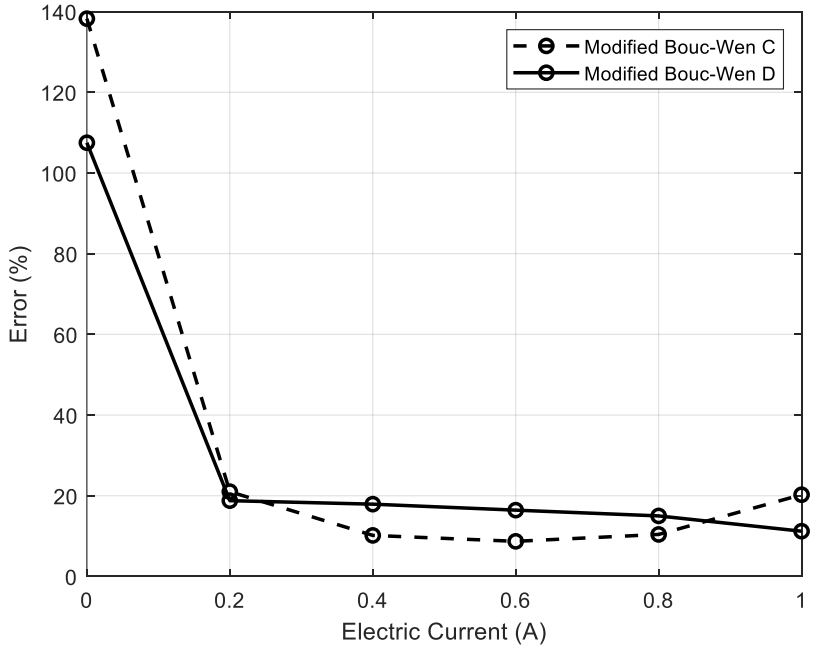

Source: Elaborated by the author

Figure 4.4 – Modified Bouc-Wen: Simulation Scenarios *A* and *B*

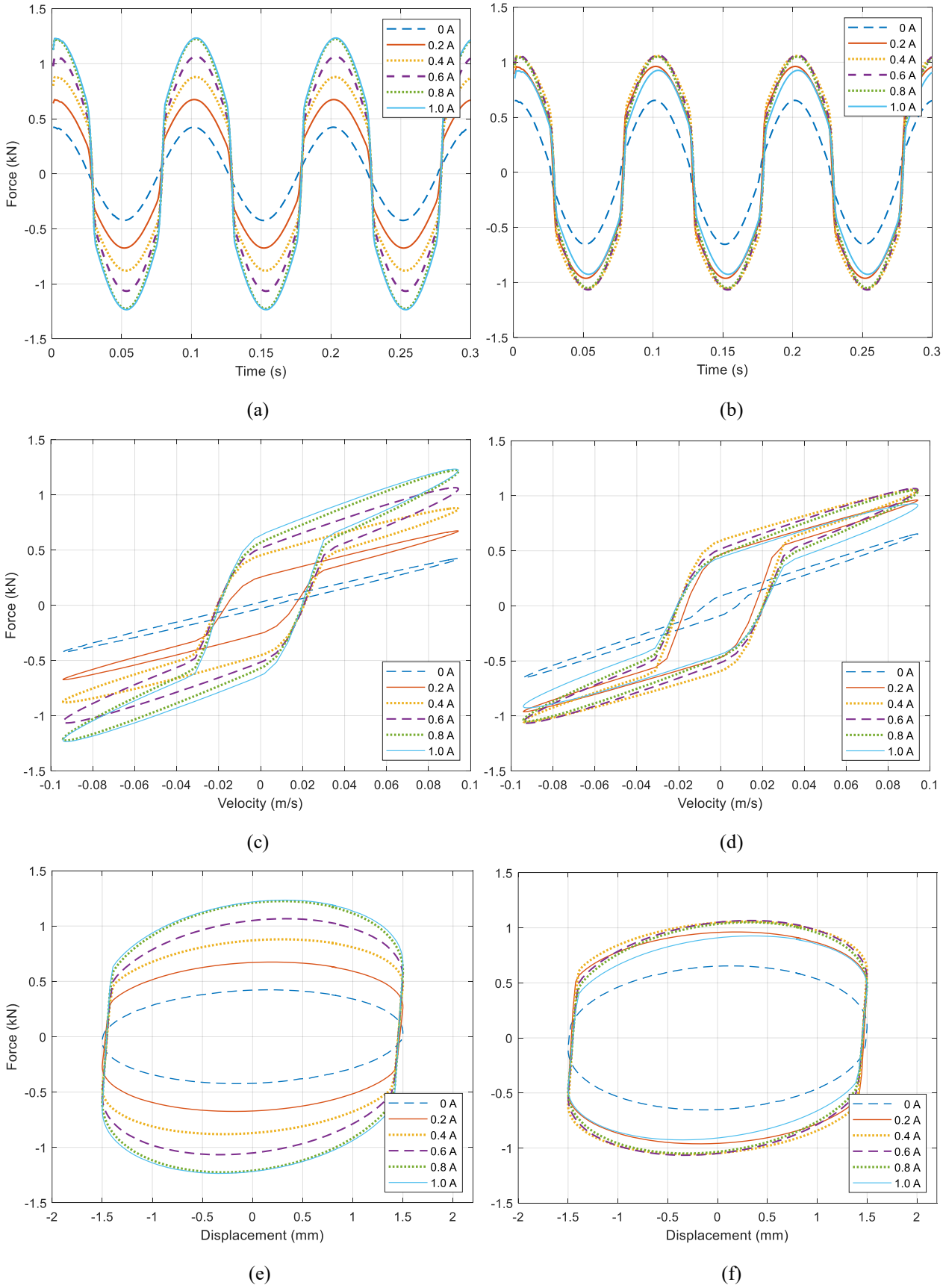

Source: Elaborated by the author

Figure 4.5 – Modified Bouc-Wen: Simulation Scenarios *C* and *D*

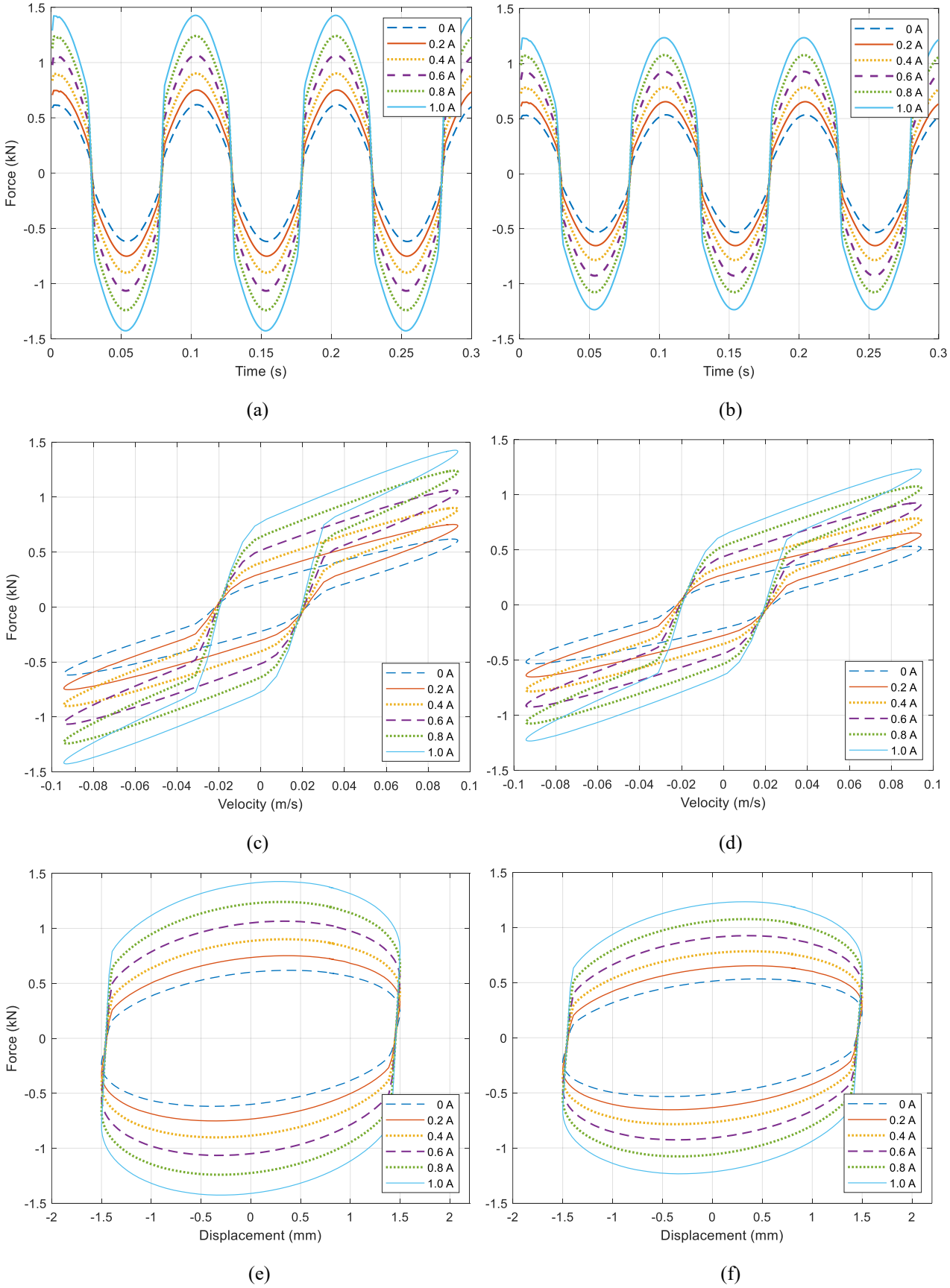

Source: Elaborated by the author

4.3.2 Hysteretic Model

Table 4.5 – Search Space for the optimized parameters in Hysteretic Model

Parameter	c_a	k_a	α_a	α_c	δ_a	f_{0a}
lower	0	-1000000	-3000	-100	0	-50
upper	6000	10	3000	100	1	50
Parameter	c_b	k_b	α_b	β	δ_b	f_{0b}
lower	-4000	0	-10000.0	-100.0	0	-100
upper	4000	1000	100000.0	100.0	1	100

Source: Elaborated by the author

The parameter updating results for the Hysteretic model are exposed in Table 4.6. In the optimization, it was considered a maximum of 40 generations for the 12 variables, a population size of 800 individuals, 0.5 for mutation, and 0.8 for crossover probability.

Table 4.6 – Parameters for hysteretic model

	0 A	**0.2 A**	**0.4 A**	**0.6 A**	**0.8 A**	**1.0 A**
c_a	3078.41	1625.78	2035.00	1711.07	672.03	363.69
c_b	1592.15	1492.85	1010.80	1184.96	1971.24	485.64
k_a	-288040.52	27.62	-40561.77	-63913.90	-77296.85	-98311.31
k_b	998.22	407.80	105.62	232.57	351.89	263.79
α_a	820.98	-595.39	-717.86	764.71	-1290.97	-1380.42
α_b	73160.81	2729.33	1931.06	745.17	2308.57	2500.17
α_c	100.00	-87.63	12.51	97.60	-56.29	43.34
β	44.38	47.39	36.32	31.38	29.93	26.88
δ_a	0.59	0.52	0.52	0.55	0.56	0.39
δ_b	0.84	0.93	0.71	0.55	0.50	0.49
f_{0a}	3.25	22.15	0.31	-4.17	13.27	0.05
f_{0b}	-8.24	44.73	-18.64	35.41	-13.35	-13.84

Source: Elaborated by the author

The obtained errors for all simulation scenarios are in Table 4.7. It is observed that, for zero electric current, hysteretic model is more representative than modified Bouc-Wen. However, the parameter fitting is also performed in function of electric current, as displayed in Equation 2.20, and error values can be more expressive for small values of electric current.

The errors obtained in scenario *A* are smaller for Hysteretic model than for modified Bouc-Wen. The model represents better the damper dynamics in all the steps of electric current analyzed. It's important to note that such a model has fewer parameters to be updated, which makes it easier to deal numerically, and its equation of motion is simpler compared to other models.

The hysteretic model has some significant disadvantages compared to the previous studied model. Figure 4.7 shows the results obtained for the simulations of scenarios *A* and *B*. In scenario *B*, there is 4722.83 % of error for 0 A. Such a value is so high that makes impossible to visualize the other steps of electric current in Figure 4.7b other than for 0 A. That happens due to high values of stiffness obtained at optimization. Reviewing the stiffness parametrization in Equation 2.20, $k = k_a \cdot i + k_b$. For $i = 0$, $k_a = -288040.52$ N/m has no influence on stiffness. It causes the high value of k_b to increase the stiffness and consequently high values of damping force are calculated. The error value for 0.2 A is also higher compared to values from 0.4 A onwards. Figure 4.8 shows the scenario *C* without the curves for 0 A. It shows that the model can predict well the damping force behavior when is not adjusted for small values of electric current.

Table 4.7 – Errors compared to experiment for Hysteretic Model

	0 A	**0.2 A**	**0.4 A**	**0.6 A**	**0.8 A**	**1.0 A**
error^A	6.82 %	10.01 %	3.50 %	6.05 %	3.09 %	3.51 %
error^B	4722.83 %	65.43 %	13.04 %	6.05 %	5.63 %	8.84 %
error^C	24.89 %	35.98 %	21.61 %	6.05 %	21.58 %	54.93 %
error^D	65.36 %	15.08 %	5.24 %	8.84 %	4.85 %	3.51 %

Source: Elaborated by the author

Hysteretic model's ability to predict better than modified Bouc-Wen the dynamics at 0 A makes the standard deviations at scenarios *C* and *D* to be smaller, with values of 16.5 % and 24.0 % of error, respectively. But, depending on the selected electric current for parameter

fitting, the mean error can be significantly different. Scenario *C* has 27.5 % of mean error while scenario *D* has 17.1 %. This means that even if hysteretic model is more precise independent of the parameter fitting criteria, the model's accuracy is impacted by that. Figure 4.9 shows graphical representations of simulation scenarios *C* and *D*, and it can be seen that the gap between the curves is larger for scenario *C*. Figure 4.6 shows Hysteretic model errors from scenarios *C* and *D*.

The smallest error obtained in scenario C was 6.05 % at 0.6 A (selected value for optimization) and the smallest for scenario *D* was 3.51 % at 1.0 A (selected value for optimization). The error increases as the electric current value distances itself from the selected one for the parameter fitting process, but not proportionally as modified Bouc-Wen model did. That occurs due to the hysteretic variable *z*, that multiplies the scale factor α in Equation 2.17, be modeled as a hyperbolic tangent which is an exponential function of parameters, as exposed in Equation 4.3.

$$\mathrm{z} = \tanh\left(\beta\dot{x} + \delta sign(x)\right) = \frac{e^{\beta\dot{x}+\delta sign(x)} - e^{-(\beta\dot{x}+\delta sign(x))}}{e^{\beta\dot{x}+\delta sign(x)} + e^{-(\beta\dot{x}+\delta sign(x))}} \tag{4.3}$$

Figure 4.6 – Comparison of errors between scenarios *C* and *D* (Hysteretic)

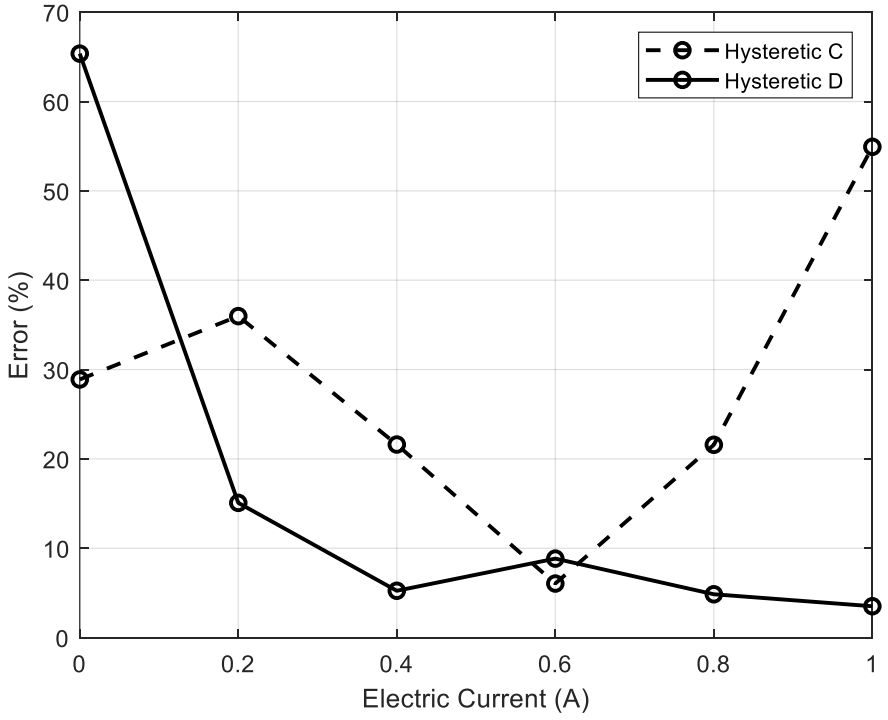

Source: Elaborated by the author

Figure 4.7 – Hysteretic: Simulation Scenarios *A* and *B*

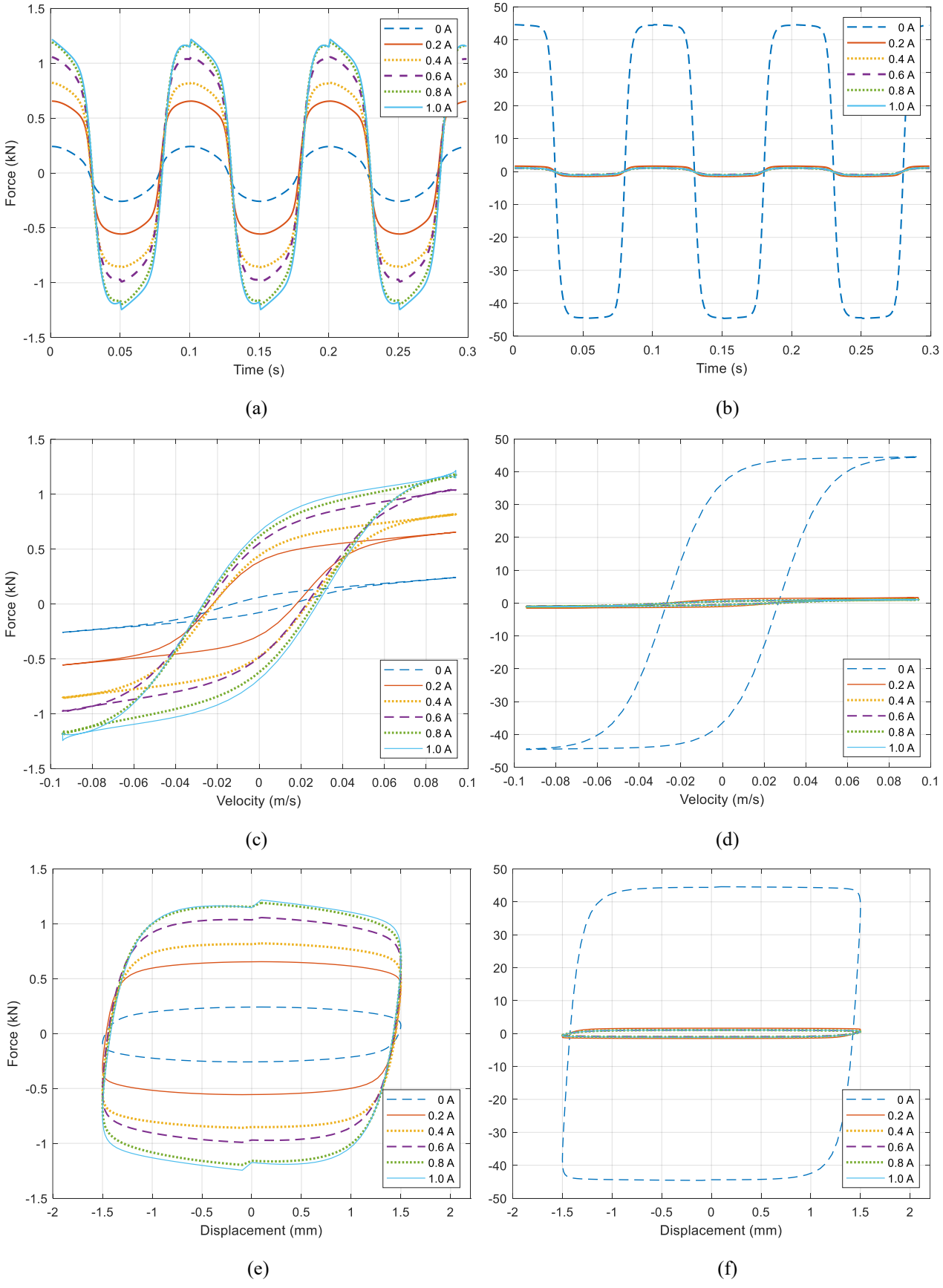

Source: Elaborated by the author

Figure 4.8 – Simulation Scenario *B* without data for i = 0 A

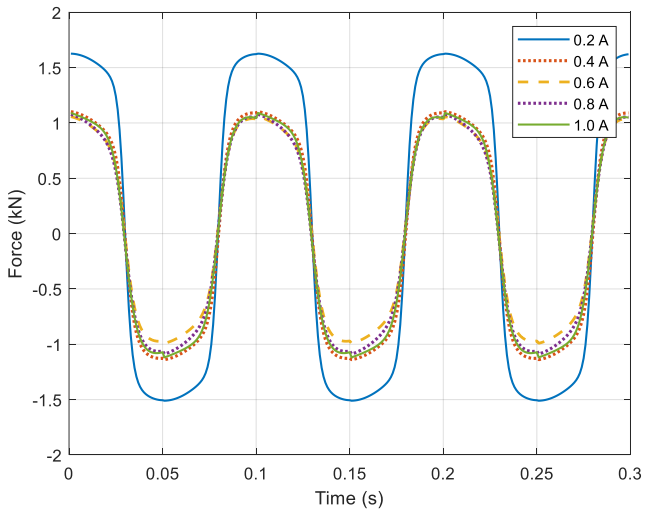

(a)

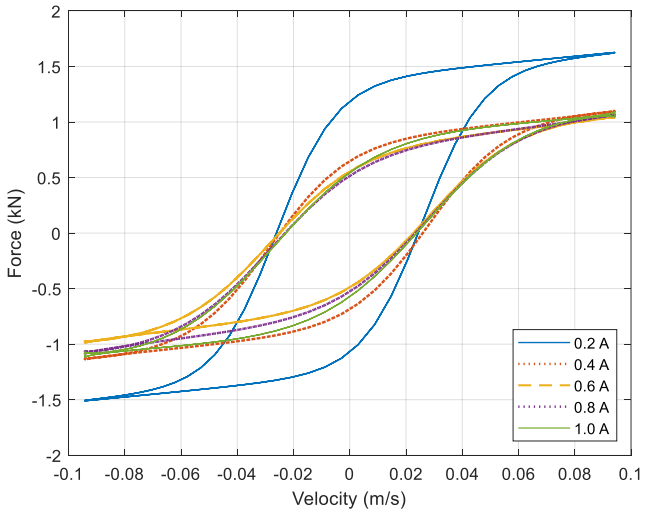

(b)

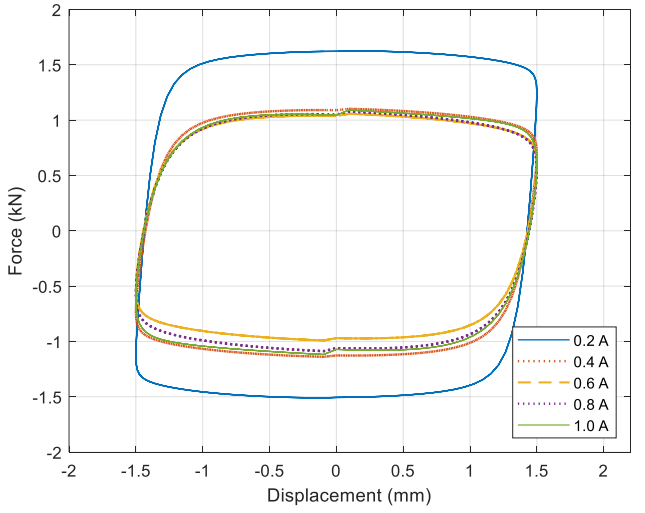

(c)

Source: Elaborated by the author

Figure 4.9 – Hysteretic: Simulation Scenarios *C* and *D*

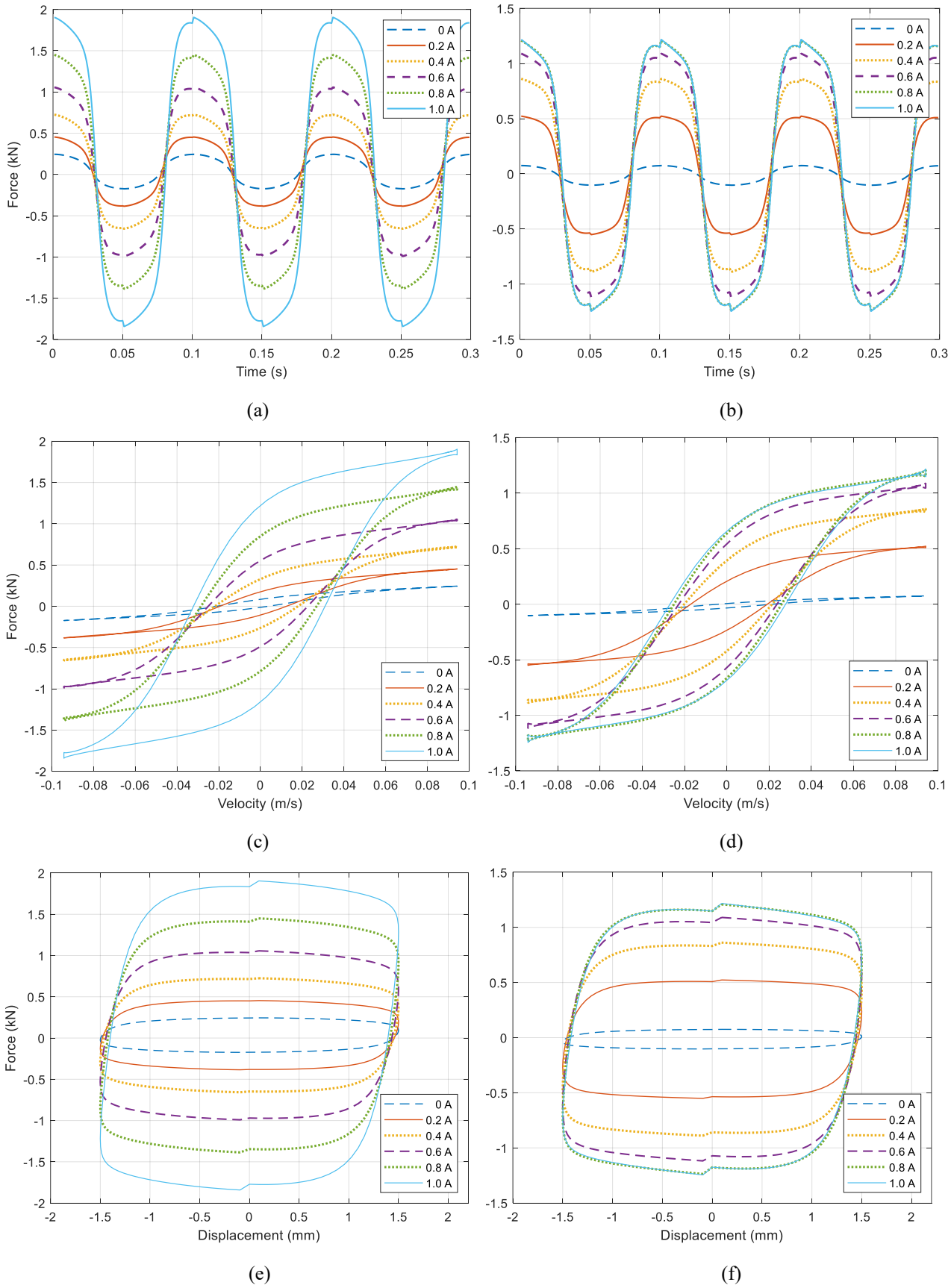

Source: Elaborated by the author

4.3.3 Fuzzy Model

Initially, six fuzzy models were developed aiming to perform a similar analysis to the one done with parametric models. For this aim, three cycles of experimental data were used as training data. The displacement and velocity for each electric current were set as the inputs for the ANFIS. The velocity data was obtained from a differentiation of displacement in time. Thus, the experimental values of damping force were set as the output training data.

The neuro-fuzzy platform used was ANFIS from Mathworks©. Three membership functions were created for each input parameter: small, moderate and large for displacement and low, moderate and high for velocity. The selected shape for input membership functions was gaussian and the inference method used was Takagi-Sugeno. This way, the consequent terms were modeled as constants, *i.e.*, $z_i = p_i x + q_i y + r_i$ with $p_i = 0$ and $q_i = 0$.

The rule set was created combining all possibilities for the membership functions for small, moderate or large values of displacement and low, moderate or high values of velocities. Such a procedure resulted in 9 rules, as exposed in Table 4.8.

Table 4.8 – Rule set

Rule	Description
1	IF (displacement is small AND velocity is low) THEN (Force is z_1)
2	IF (displacement is small AND velocity is moderate) THEN (Force is z_2)
3	IF (displacement is small AND velocity is high) THEN (Force is z_3)
4	IF (displacement is moderate AND velocity is low) THEN (Force is z_4)
5	IF (displacement is moderate AND velocity is moderate) THEN (Force is z_5)
6	IF (displacement is moderate AND velocity is high) THEN (Force is z_6)
7	IF (displacement is large AND velocity is low) THEN (Force is z_7)
8	IF (displacement is large AND velocity is moderate) THEN (Force is z_8)
9	IF (displacement is large AND velocity is high) THEN (Force is z_9)

Source: Elaborated by the author

ANFIS platform allows the user to select the optimization technique between *backpropagation* and *hybrid*. The first option uses backpropagation for all parameters and the second uses backpropagation for the parameters associated with input membership functions and least squares estimation for the parameters associated with the output membership functions (ROGER; GULLEY, 1997).

According to Nedjah and Mourelle (2005), Takagi-Sugeno neuro-fuzzy systems learn the membership functions using backpropagation and least square estimation to determine the coefficients of the linear combinations in the rules' conclusion. Based on that, the *hybrid* option was selected for the optimization technique at ANFIS platform. The obtained parameters after training are exposed in Tables 4.9 to 4.11, and since a gaussian shape was selected for the membership functions, the parameters are mean and standard deviation. Table 4.9 shows mean and standard deviation values for displacement, Table 4.10 shows mean and standard deviation values for velocity, and Table 4.11 shows the values of z_i for each rule.

In simulation scenario *A*, the deviation from experimental data was small for all electric current analyzed. But it is important to stand out that, in this case, there are six fuzzy models trained for six different conditions of electric current. This is the reason these models were tested for the same electric current of 0.6 A in scenario *B*.

Table 4.9 – Displacement (mm) parameters after training

	Small		**Moderate**		**Large**	
i	$\bar{x}$	σ	$\bar{x}$	σ	$\bar{x}$	σ
0 A	-2.0430	0.2183	0.1188	1.1280	2.4130	0.4285
0.2 A	-2.4100	0.3723	0.1509	1.2340	2.7750	0.5407
0.4 A	-2.6540	0.4646	0.05489	1.279	2.729	0.5397
0.6 A	-2.5300	0.4013	0.1157	1.215	2.712	0.5441
0.8 A	-2.516	0.398	0.07672	1.154	2.632	0.5459
1.0 A	-2.485	0.3889	0.09975	1.154	2.653	0.5379

Source: Elaborated by the author

Table 4.10 – Velocity (mm/s) parameters after training

	Low		**Moderate**		**High**	
i	$\bar{x}$	σ	$\bar{x}$	σ	$\bar{x}$	σ
0 A	-94.96	40.44	-0.133	40.34	94.73	40.45
0.2 A	-95.50	40.63	-0.1608	40.46	95.24	40.62
0.4 A	-94.91	40.66	0.4397	40.49	95.79	40.69
0.6 A	-95.79	4..85	-0.137	40.63	95.58	40.91
0.8 A	-94.91	40.62	0.1033	40.35	95.15	40.72
1.0 A	-94.99	40.88	0.6327	40.6	96.32	40.98

Source: Elaborated by the author

Table 4.11 – Force (kN) parameters after training

	0 A	0.2 A	0.4 A	0.6 A	0.8 A	1.0 A
z_1	-2.478	-10.48	-21.46	-22.61	-21.02	-25.7
z_2	-0.4114	-2.334	-4.326	-3.646	-3.176	-3.475
z_3	5.856	13.22	13.98	17.12	13.12	14.27
z_4	-0.2496	-0.6297	-0.8813	-1.06	-1.221	-1.25
z_5	-0.105	-0.2414	-0.216	-0.4557	-0.5729	-0.5599
z_6	0.2769	0.6782	0.9293	1.135	1.311	1.359
z_7	-0.1904	-4.253	-3.146	-0.8345	0.07375	0.8384
z_8	0.7359	5.176	4.956	5.753	4.9	5.29
z_9	5.371	22.56	21.88	25.23	18.83	26.23

Source: Elaborated by the author

Table 4.12 shows the calculated errors for both scenarios. As expected, at 0.6 A, the error is the same. However, for the other steps of electric current, it drastically increases in scenario *B*. Fuzzy models were not able to predict the dynamics of other values of electric current without a previous training. It can be graphically observed in Figure 4.10. Scenario *A* seems to display acceptable results as shown in parts *a*, *c* and *e*. But the curves should be overlapped, or close to it, in scenario *B* and that is not what happens as can be seen in parts *b*, *d* and *f*.

Table 4.12 – Errors in scenarios *A* and *B*

Current	0 A	0.2 A	0.4 A	0.6 A	0.8 A	1.0 A
$\mathbf{error}^{A}$	5.12 %	4.11 %	3.25 %	3.48 %	2.78 %	3.67 %
$\mathbf{error}^{B}$	77.10 %	39.36 %	16.67 %	3.48 %	16.03 %	19.32 %

Source: Elaborated by the author

The curves from scenarios *A* and *B* were overlapped in Figure 4.11 to qualitatively analyze how different they are. It is possible to observe that they are very close to each other. This indicates that, for the selected setup, fuzzy models need to be trained for the conditions that the analysis will be performed. For this reason, simulations scenarios *C* and *D*, similar to the parametric models' study, were not performed in this case since it is already observed that the models need more information to predict the MR damper behavior in different conditions. Instead, another input variable was added to the model and it seemed to be a better option, as will be presented next.

Figure 4.10 – Fuzzy: Simulation Scenarios *A* and *B*

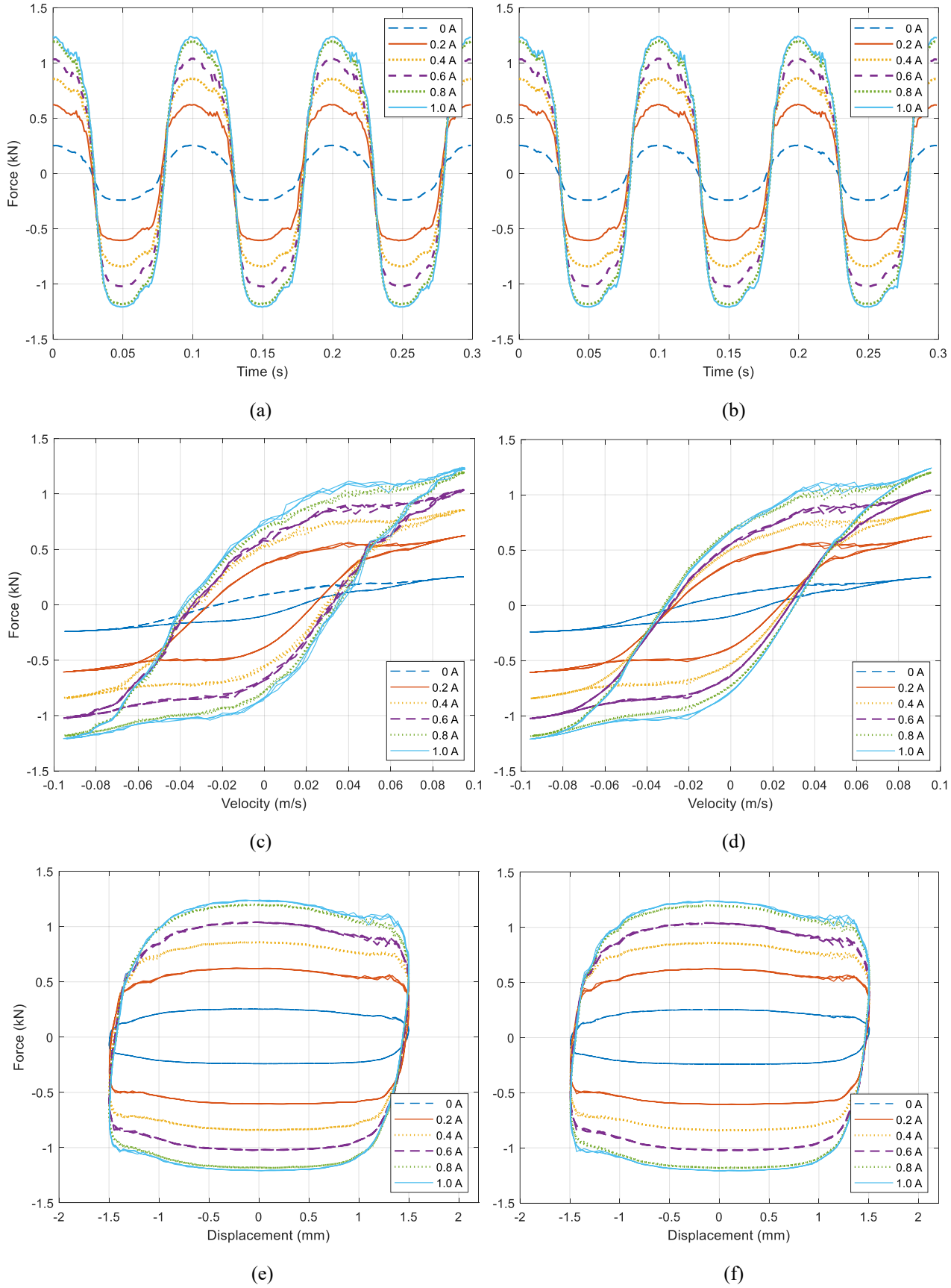

Source: Elaborated by the author

Figure 4.11 – Fuzzy: Overlapped data from Simulation Scenarios *A* and *B*

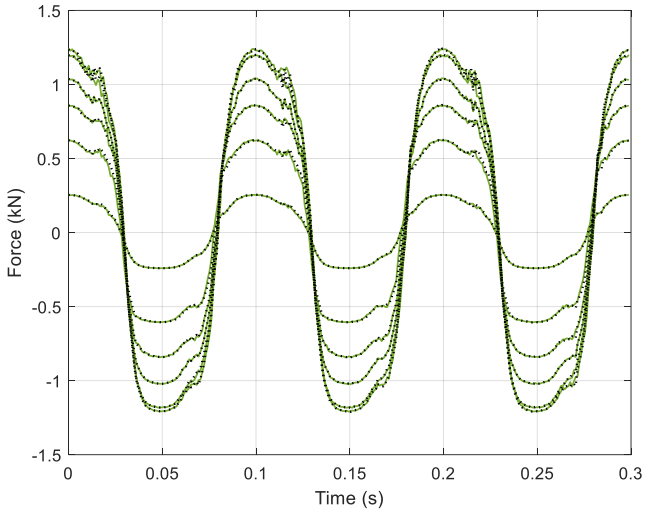

(a)

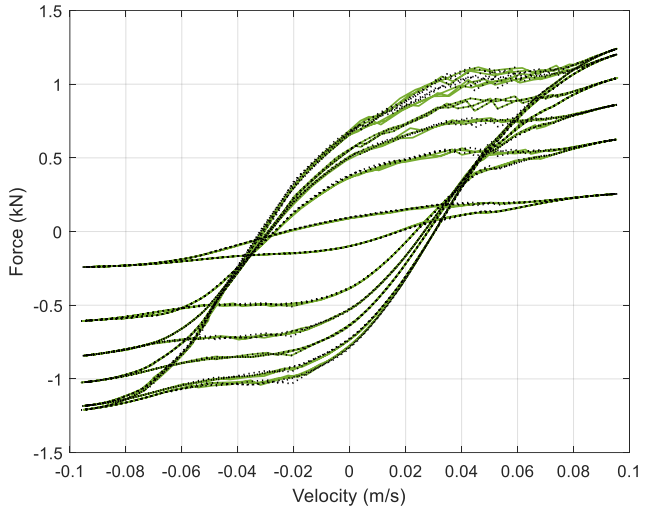

(b)

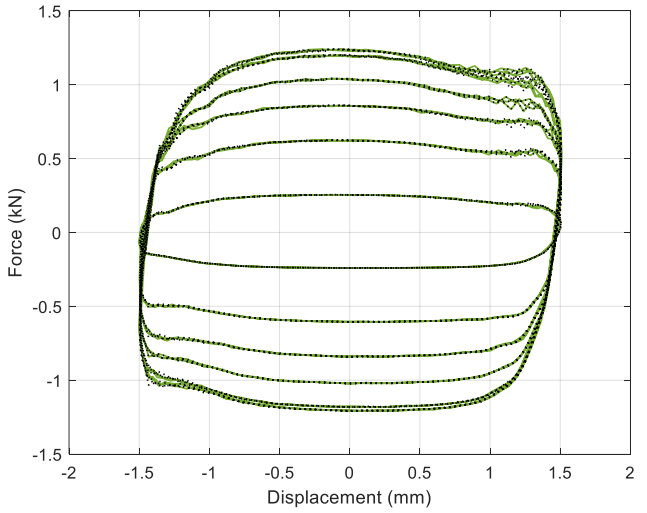

(c)

Source: Elaborated by the author

Now, one single fuzzy model capable of predict the MR damper's dynamic behavior was developed. Similarly, three cycles of experimental data were used as training data. In this case, the electric current was added as an input to the model alongside with displacement and velocity, and damping force was the output.

The same neuro-fuzzy platform was used. Three membership functions were created for each input parameter: small, moderate and large for displacement and low, moderate and high for velocity and electric current. The membership functions have gaussian shape and the inference method used is Takagi-Sugeno. The consequent terms were modeled the same way: $z_i = p_i x + q_i y + r_i$ with $p_i = 0$ and $q_i = 0$.

The rule set was created following the same procedure as before: all possible combinations of small, moderate or large values of displacement and low, moderate or high values of velocities and electric currents for the membership functions. Adding electric current as an input increased the number of possible combinations and consequently the number of rules. Table 4.13 presents the set of 27 rules considered in the model.

Table 4.13 – Rule set (continued)

Rule	Description
1	IF (current is low AND displacement is small AND velocity is low) THEN (Force is z_1)
2	IF (current is low AND displacement is small AND velocity is moderate) THEN (Force is z_2)
3	IF (current is low AND displacement is small AND velocity is high) THEN (Force is z_3)
4	IF (current is low AND displacement is moderate AND velocity is low) THEN (Force is z_4)
5	IF (current is low AND displacement is moderate AND velocity is moderate) THEN (Force is z_5)
6	IF (current is low AND displacement is moderate AND velocity is high) THEN (Force is z_6)
7	IF (current is low AND displacement is large AND velocity is low) THEN (Force is z_7)
8	IF (current is low AND displacement is large AND velocity is moderate) THEN (Force is z_8)
9	IF (current is low AND displacement is large AND velocity is high) THEN (Force is z_9)
10	IF (current is moderate AND displacement is small AND velocity is low) THEN (Force is z_{10})
11	IF (current is moderate AND displacement is small AND velocity is moderate) THEN (Force is z_{11})
12	IF (current is moderate AND displacement is small AND velocity is high) THEN (Force is z_{12})
13	IF (current is moderate AND displacement is moderate AND velocity is low) THEN (Force is z_{13})
14	IF (current is moderate AND displacement is moderate AND velocity is moderate) THEN (Force is z_{14})
15	IF (current is moderate AND displacement is moderate AND velocity is high) THEN (Force is z_{15})
16	IF (current is moderate AND displacement is large AND velocity is low) THEN (Force is z_{16})
17	IF (current is moderate AND displacement is large AND velocity is moderate) THEN (Force is z_{17})
18	IF (current is moderate AND displacement is large AND velocity is high) THEN (Force is z_{18})
19	IF (current is high AND displacement is small AND velocity is low) THEN (Force is z_{19})

Table 4.13 – Rule set (end)

Rule	Description
20	IF (current is high AND displacement is small AND velocity is moderate) THEN (Force is z_{20})
21	IF (current is high AND displacement is small AND velocity is high) THEN (Force is z_{21})
22	IF (current is high AND displacement is moderate AND velocity is low) THEN (Force is z_{22})
23	IF (current is high AND displacement is moderate AND velocity is moderate) THEN (Force is z_{23})
24	IF (current is high AND displacement is moderate AND velocity is high) THEN (Force is z_{24})
25	IF (current is high AND displacement is large AND velocity is low) THEN (Force is z_{25})
26	IF (current is high AND displacement is large AND velocity is moderate) THEN (Force is z_{26})
27	IF (current is high AND displacement is large AND velocity is high) THEN (Force is z_{27})

Source: Elaborated by the author

The neuro-fuzzy optimization technique used was also backpropagation for parameters corresponding with inputs and least squares for parameters corresponding with the output. After training, values of mean and standard deviation for electric current, displacement, velocity and damping force were obtained. They are displayed in Tables 4.14 to 4.17, respectively.

Table 4.14 – Electric current (A) parameters after training

Low		Moderate		High	
$\bar{x}$	σ	$\bar{x}$	σ	$\bar{x}$	σ
-0.09468	0.1867	0.3549	0.2069	0.9048	0.3245

Source: Elaborated by the author

Table 4.15 – Displacement (mm) parameters after training

Small		Moderate		Large	
$\bar{x}$	σ	$\bar{x}$	σ	$\bar{x}$	σ
-2.088	0.3057	0.04375	1.106	2.143	0.4329

Source: Elaborated by the author

Table 4.16 – Velocity (mm/s) parameters after training

Low		Moderate		High	
$\bar{x}$	σ	$\bar{x}$	σ	$\bar{x}$	σ
-95.84	40.93	0.2862	40.85	96.44	40.94

Source: Elaborated by the author

Table 4.17 – Force (kN) parameters after training

z_1	0.1840	z_{10}	-4.8470	z_{19}	-7.0650
z_2	0.2143	z_{11}	-1.3080	z_{20}	-1.3760
z_3	0.2072	z_{12}	6.7230	z_{21}	5.2260
z_4	-0.08422	z_{13}	-0.7713	z_{22}	-1.2610
z_5	-0.0461	z_{14}	-0.2894	z_{23}	-0.6149
z_6	0.09722	z_{15}	0.8422	z_{24}	1.3780
z_7	0.01684	z_{16}	-1.9590	z_{25}	-1.0790
z_8	-0.003367	z_{17}	1.3540	z_{26}	2.0500
z_9	0.4448	z_{18}	4.4490	z_{27}	7.7990

Source: Elaborated by the author

Table 4.18 shows the calculated errors for the proposed fuzzy model. The model was capable to predict well the dynamic behavior at all the analyzed steps of electric current, having errors smaller than 7 %. That accredit more robustness to the non-parametric modeling than to the parametric approach, *i.e.*, the output damping force is more accurate in a model that also has precision. The error is greater at 0 A and 0.2 A with 6.40 % and 5.36 %, respectively. The best fit results are at 0.8 A with 3.24 % of deviation from experiment. This is smaller than the smallest value obtained in hysteretic model: 3.51 % for 1.0 A in scenario *D*. Furthermore, the mean error for fuzzy model is 4.6 % while the standard deviation of errors is 1.1 % what confirms the robustness of this fuzzy model to describe the MR damper in the studied conditions of displacement, frequency and electric current.

Table 4.18 – Error between fuzzy model and experimental data

Current	**0 A**	**0.2 A**	**0.4 A**	**0.6 A**	**0.8 A**	**1.0 A**
error	6.40 %	5.36 %	4.23 %	4.13 %	3.24 %	4.10 %

Source: Elaborated by the author

Figure 4.12 represents the proposed fuzzy model graphically. Numerical data was overlapped with experimental values. Figure 4.12a presents the curves of damping force versus time, Figure 4.12b presents the curves of damping force versus velocity, and Figure 4.12c presents values of damping force versus displacement. The dotted curves correspond to experimental data and the continuous curves are from numerical fuzzy calculations.

Figure 4.12 – Proposed fuzzy model overlapped to experimental data

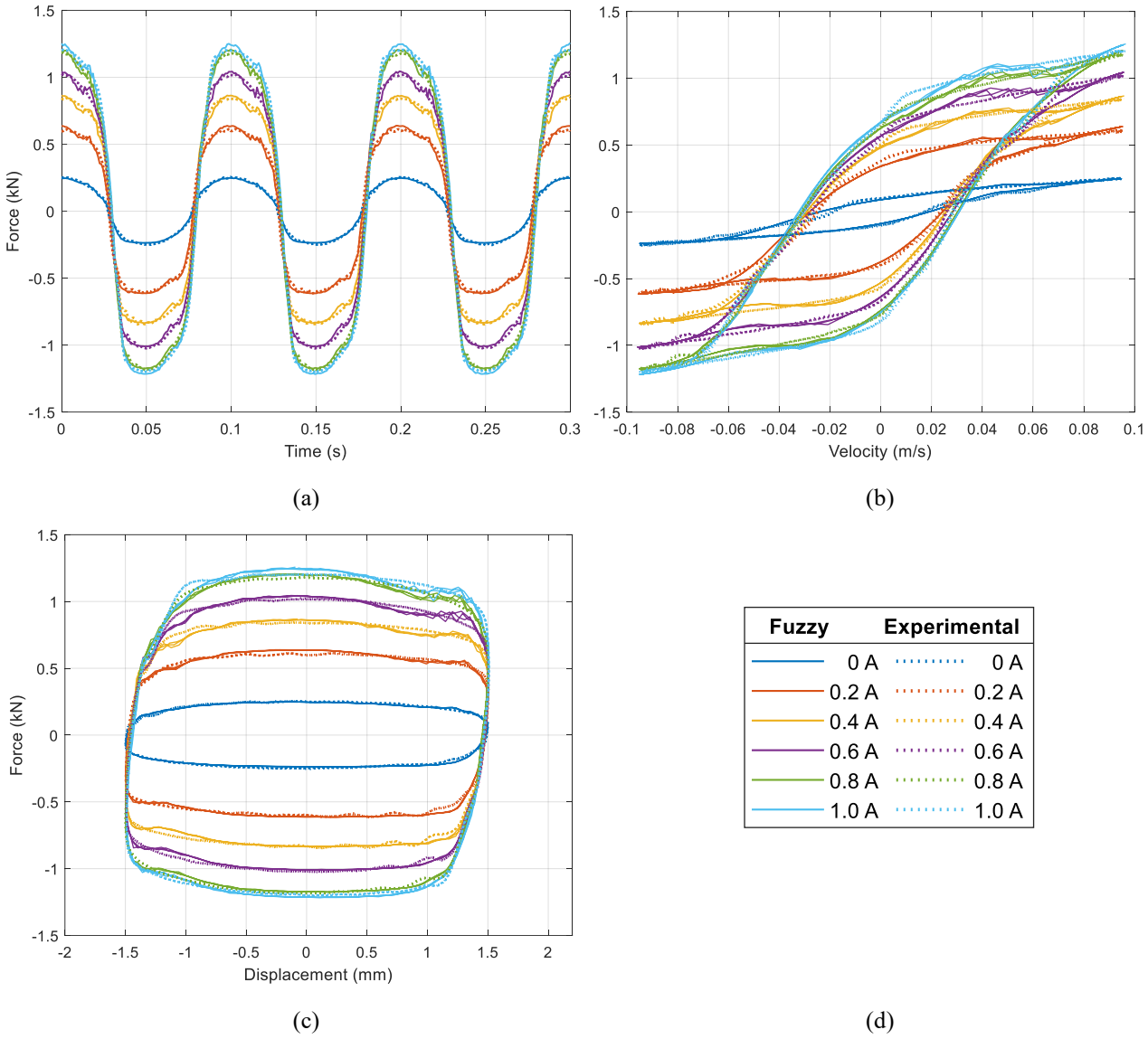

Source: Elaborated by the author

Figure 4.13 brings a visual comparison of experimental and numerical values. Modified Bouc-Wen model, hysteretic model, the proposed fuzzy model, and the experimental data are overlapped for 0.6 A. It is possible to see the differences between each curve, especially at damping force versus velocity where such differences become more evident. Modeling MR dampers using hyperbolic tangent, the strategy of hysteretic model, seemed an accurate and simple way. The disadvantages rely on the parametrization in function of electric current which increase errors next to zero and affect the model's performance depending on the region of parameter fitting. Neuro-fuzzy modeling has the accuracy and precision, needing only to be trained for the desired application.

Figure 4.13 – Comparison between the models and experimental data (i = 0.6 A; f = 10 Hz)

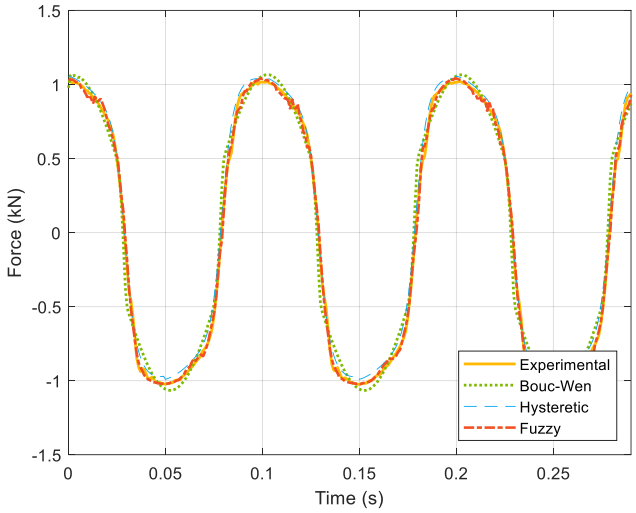

(a)

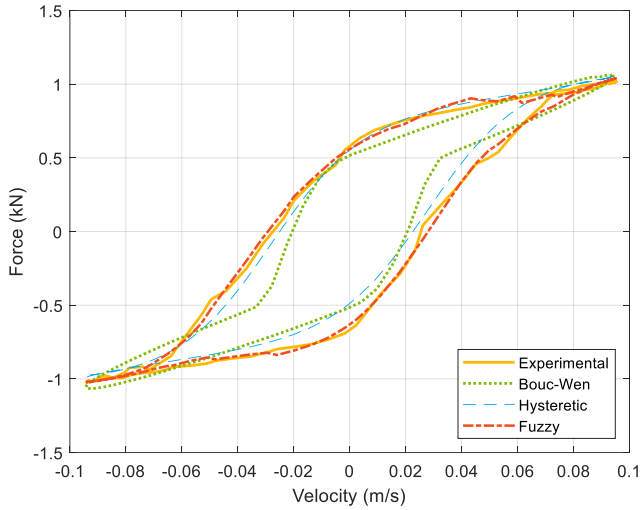

(b)

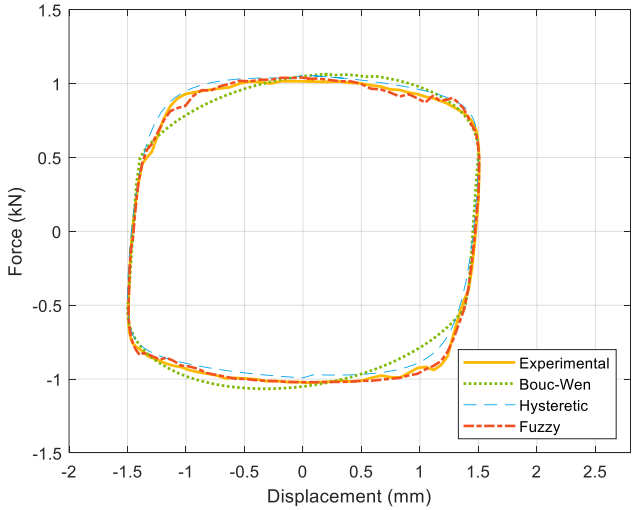

(c)

Source: Elaborated by the author

Errors from simulation scenarios *C* and *D* of modified Bouc-Wen and hysteretic models are displayed graphically alongside with errors from fuzzy model in Figure 4.14. Black circled points correspond to modified Bouc-Wen where points linked by a dashed line are from scenario *C* and points linked by a continuous line are from scenario *D*. Similarly, green points with triangles correspond to hysteretic model's errors where points linked by a dashed line are from scenario *C* and points linked by a continuous line are from scenario *D*. The points with blue diamonds linked by a dashed line correspond to errors from proposed fuzzy model.

Figure 4.14 – Errors for Modified Bouc-Wen, Hysteretic and Fuzzy models

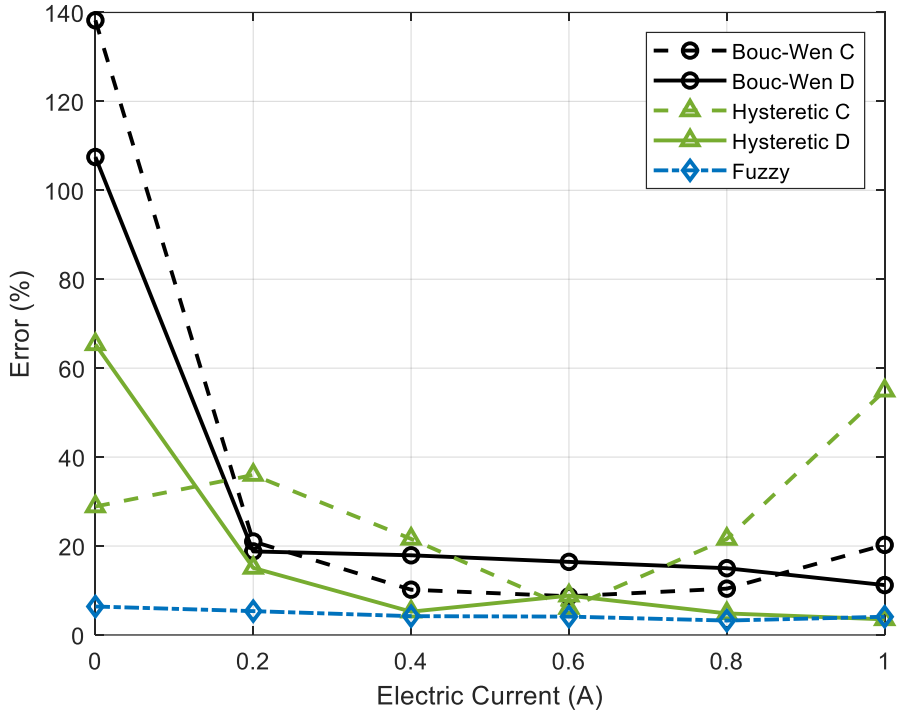

Source: Elaborated by the author

Such a way of expressing errors gives a good measure for comparing the difference between models. It ratifies the observed precision of modified Bouc-Wen that predicted the MR damper behavior in a similar way for both optimization setups. The eficiency of hysteretic model to obtain accurate values at parameter fitting is also highlighted, with small errors, except for 0 A and 0.2 A. Finally, the fuzzy model ability to predict well the MR damper's dynamics in all the analyzed points makes it a good alternative to this application.

CHAPTER V

CONCLUSION

"Open mind for a different view and nothing else matters."
– Metallica

A methodology for developing a fuzzy model for magnetorheological dampers was presented in this work. The non-parametric approach aims to simplify the modeling procedure. MR dampers have hydrodynamic, thermodynamic and magnetic coupled phenomena what is complex to model in function of parameters. A general overview of smart materials was presented at Chapter 1. The required concepts and definitions for the comprehension and development of such a model were explored with a vast literature review in the next two chapters.

In Chapter 2, it was given a notion of what magnetorheological dampers and magnetorheological fluids are and its applications. Mathematical models with parametric equations available in literature were presented. The parametrization techniques were also detailed in that chapter. In Chapter 3, the concepts related to fuzzy sets were displayed with playful examples and mathematical expressions easy to understand. Initially, the classical fuzzy approach was defined, *i.e.*, the definition of fuzzy sets, membership functions, grade of membership and operations with fuzzy sets were addressed. Then, fuzzy rule-based systems definitions were explored to finally explain how artificial neural networks are applied in fuzzy logic with neuro-fuzzy. A brief overview of the optimization techniques used in this work were also addressed at the end of Chapter 3.

Chapter 4 was designed to deal with methodology. Amid the mathematical models presented in Chapter 2, two of them were selected for analysis: the modified Bouc-Wen model and the Hysteretic model. Four scenarios of simulations were performed with different parameter fitting values. The optimization was done using differential evolution algorithm with

an objective function that minimized the normalized errors between numerical and experimental data. The experimental values used were obtained from a previous research developed at Laboratory of Mechanics and Structures (LMEst). Modified Bouc-Wen model was more precise and less accurate than hysteretic model. Parametric models were not capable to predict the damping force when optimized for zero or almost zero values of electric current, especially hysteretic model which had errors greater than 1000 %.

Then, it was shown that a similar analysis could not be performed with neuro-fuzzy model due to its dependence of training data to different steps of electric current. Considering electric current, displacement and velocity as inputs, the model was able to predict well the damping force at all steps of electric current.

5.1 Main contributions

This work is a continuation of a previous research developed at LMEst that now can be more explored both at UFU and other universities. This dissertation serves as a good source of knowledge about MR dampers and fuzzy logic with the text and the relevant bibliographical references.

The analysis made in chapter 4, forcing the models to fail to predict the damping force, can inspire researchers from other fields to apply the same approach to their work and take a broader view of the data they are eventually managing. Thus, this text documents how two of the best parametric models of MR dampers predict the damping force in different conditions.

All models studied in this work can be replicated since the necessary parameter values are all expressed in tables. That makes possible the readers to exercise numerical skills, criticize this work, find leaks and help to develop science even more.

5.2 Future works

Studies about magnetorheological dampers, fuzzy sets and applications can be carried out in the future. For example, applying MR dampers to a rotating machine bench and characterizing it numerically and experimentally can yield interesting results to compare to the traditional vibration control options.

Other possibility is to perform an experimental characterization of a MR damper sweeping different ranges of frequency and displacement. The same methodology presented in this work can be used and the results compared.

The uncertainties intrinsic to the system can be treated statistically to have quantified comparison between models. Thus, different optimization techniques for parameter fitting and different inference methods for the fuzzy model can be implemented to analyze the impact of these variables on computational cost.

Moreover, a non-parametric model based on deep learning can also be an alternative for modeling MR dampers. Such a model could have an artificial neural network with more layers and nodes than neuro-fuzzy.

Developing a brand-new model of magnetorheological damper or fluid and starting a national mass production of this technology is the final suggestion of future work. The range of applications is wide and it would generate not only comfort and safety but profit and jobs.

5.3 Final thoughts

Magnetorheological dampers are a good alternative for semi-active vibration control. In that context, it is important to have reliable and robust models. This works' main goal was to develop a fuzzy model able to predict the dynamic behavior of a MR damper with the available data. That objective was successfully achieved with satisfactory results. This makes possible to future researchers and engineers to improve performance of systems based on magnetorheological dampers and develop new product modalities to increase comfort and safety to the final users.

References

AHAMED, R; CHOI, S; FERDAUS, M. A state of art on magneto-rheological materials and their potential applications. **Journal of Intelligent Material Systems and Structures**, v. 29, n. 10, p. 2051-2095, 2018. https://doi.org/10.1177/1045389X18754350

ARAÚJO, C. J.; MONTEIRO, E. F.; REIS, R. P. B. **Sistema de caracterização de ligas com memória de forma utilizando o efeito termoelétrico**. Titular: INPI. BR n. PI 1003053-0 A2. Depósito: 09 ago. 2010. Concessão: 28 jul. 2015.

BARBOSA, P. C. P. F. **Análise do comportamento dinâmico de eixos de material composto em máquinas rotativas.** Master's thesis. Universidade Federal de Uberlândia, 2018. http://dx.doi.org/10.14393/ufu.di.2018.1121

BONISSONE, P. P. *et al*. Industrial applications of fuzzy logic at General Electric. **Proceedings of the IEEE**, v. 83, n. 3, p. 450-465, 1995. https://doi.org/10.1109/5.364490

CAVALINI JUNIOR, A. A. **Detecção e identificação de trincas transversais incipientes em eixos horizontais flexíveis de máquinas rotativas.** Doctoral dissertation. Universidade Federal de Uberlândia, 2013.

CAVALINI JUNIOR, A. A. *et al.* **Semi-active vibration control of a rotating shaft by using a magneto rheological damper.** Rio de Janeiro: COBEM, 2015.

CHEN, C. H; LIN, C. J; LIN, C. T. Nonlinear system control using adaptive neural fuzzy networks based on a modified differential evolution. **IEEE Transactions on Systems, Man, and Cybernetics, Part C (Applications and Reviews)**, v. 39, n. 4, p. 459-473, 2009. https://doi.org/10.1109/TSMCC.2009.2016572

CRIVELLARO, C. **Controle Robusto de Suspensão Semi-Ativa para Caminhonetes Utilizando Amortecedores Magneto Reológicos.** Doctoral dissertation. Universidade Federal de Minas Gerais, 2008. https://doi.org/10.11606/T.3.2008.tde-09022009-140556

DORIA, A. Framed Harvesters for Collecting Energy from Vibrations in Industrial Plants. In: **ASME 2019 International Design Engineering Technical Conferences and Computers and Information in Engineering Conference**. American Society of Mechanical Engineers Digital Collection, 2019. https://doi.org/10.1115/DETC2019-97291

DYKE, S. J. **Acceleration Feedback Control Strategies for Active and Semi-active Control Systems: Modeling, Algorithm Development, And Experimental Verification.** Doctoral dissertation. University of Notre Dame, 1996.

FRANCO, Vitor Ramos. Monitoramento da integridade em estruturas aeronáuticas. 2009.

GAMOTA, D. R.; FILISKO, F. E. Dynamic mechanical studies of electrorheological materials: moderate frequencies. **Journal of rheology**, v. 35, n. 3, p. 399-425, 1991. https://doi.org/10.1122/1.550221

HODGES, Dewey H.; PIERCE, G. Alvin. **Introduction to structural dynamics and aeroelasticity**. Cambridge University Press, 2011.

JAFELICE, R. S. M. **Modelagem fuzzy para dinâmica de transferência de soropositivos para HIV em doença plenamente manifesta**. Doctoral dissertation. Universidade Estadual de Campinas, 2003.

JANG, J.-SR. **Fuzzy controller design without domain experts.** In [1992 Proceedings] IEEE International Conference on Fuzzy Systems. IEEE, 1992. p. 289-296. https://doi.org/10.1109/FUZZY.1992.258631

KARNOPP, D; CROSBY, M. J; HARWOOD, R. A. Vibration control using semi-active force generators. **Journal of Engineering for Industry**, 1974. https://doi.org/10.1115/1.3438373

KORNMANN, X. *et al*. Active fibre composites: sensors and actuators for smart composites & structures. In: **Proceedings 11 th European Conference on Composite Materials, paper**. 2004. p. 9.

KOROISHI, E. H. **Controle de vibrações em máquinas rotativas utilizando atuadores eletromagnéticos.** Doctoral dissertation. Universidade Federal de Uberlândia, 2013.

KWOK, N. M. *et al*. A novel hysteretic model for magnetorheological fluid dampers and parameter identification using particle swarm optimization. **Sensors and Actuators A: Physical**, v. 132, n. 2, p. 441-451, 2006. https://doi.org/10.1016/j.sna.2006.03.015

LORD. **Magneto-Rheological (MR) Suspension Systems**. [201-]. Disponível em: <https://lordfulfillment.com/pdf/44/PB8140_MRSuspensionBrochure.pdf>. Acesso em: 26 de ago. de 2019.

LIU, S; TOMIZUKA, M; ULSOY, G. Strategic issues in sensors and smart structures. **Structural Control and Health Monitoring: The Official Journal of the International Association for Structural Control and Monitoring and of the European Association for the Control of Structures**, v. 13, n. 6, p. 946-957, 2006. https://doi.org/10.1002/stc.88

MAMDANI, E.H. **Advances in the linguistic synthesis of fuzzy controllers.** International Journal of Man-Machine Studies, London, v. 8, p. 669-678. 1976. https://doi.org/10.1016/S0020-7373(76)80028-4

MARANGONI, B. G. **Controle ativo de vibrações do tipo *self-sensing* utilizando atuadores eletromagnéticos.** Master's thesis. Universidade Federal de Uberlândia, 2020. http://doi.org/10.14393/ufu.di.2020.242

NEDJAH, N; MOURELLE, L. M. **Fuzzy systems engineering: theory and practice**. Springer Science & Business Media, 2005.

NIELSEN, M. A. **Neural networks and deep learning**. San Francisco, CA: Determination press, 2015.

PASCHOAL, E. F. **Controle semi-ativo de vibrações usando lógica nebulosa e fluido magnetoreológico.** Master's thesis. Universidade Estadual Paulista, 2011.

PELLETIER, F. J. Metamathematics of fuzzy logic. 2000.

PEREIRA, B. L. **Aplicação de sistemas neuro-fuzzy e evolução diferencial na modelagem e controle de veículo de duas rodas**. 2017. Master's thesis. Universidade Federal de Uberlândia, 2017. http://dx.doi.org/10.14393/ufu.di.2017.46

ROGER, J. S.; GULLEY, Jang Ned. **MATLAB: Fuzzy Logic Tool Box.** 1997.

RUGGIERO, M. A. G.; LOPES, V. L. R. **Cálculo numérico: aspectos teóricos e computacionais**. Makron Books do Brasil, 1997.

SANT'ANA, V. T. **Aerodynamic Modeling using Neuro-Fuzzy for a scaled model of Cessna 182**. 2019. 102 p. Master's thesis. Universidade Federal de Uberlândia, 2019. http://dx.doi.org/10.14393/ufu.di.2019.2176

SCHURTER, K. C.; ROSCHKE, P. N. Fuzzy modeling of a magnetorheological damper using ANFIS. In: **Ninth IEEE International Conference on Fuzzy Systems. FUZZ-IEEE 2000 (Cat. No. 00CH37063)**. IEEE, 2000. p. 122-127. https://doi.org/10.1109/FUZZY.2000.838645

SCHWARTZ, M. **Encyclopedia of smart materials, 2 volume set**. 2002.

SHERMAN, S. G.; BECNEL, A. C.; WERELEY, N. M. Relating Mason number to Bingham number in magnetorheological fluids. **Journal of Magnetism and Magnetic Materials**, v. 380, p. 98-104, 2015. https://doi.org/10.1016/j.jmmm.2014.11.010

SIMÕES, M. G; SHAW, I. S. **Controle e modelagem fuzzy**. Editora Blucher, 2007.

SPENCER JR, B. F. *et al*. Phenomenological model for magnetorheological dampers. **Journal of engineering mechanics**, v. 123, n. 3, p. 230-238, 1997. https://doi.org/10.1061/(ASCE)0733-9399(1997)123:3(230)

STANWAY, R. S. J. L.; SPROSTON, J. L.; STEVENS, N. G. Non-linear modelling of an electro-rheological vibration damper. **Journal of Electrostatics**, v. 20, n. 2, p. 167-184, 1987. https://doi.org/10.1016/0304-3886(87)90056-8

SUGANTHI, L.; INIYAN, S.; SAMUEL, A. A. Applications of fuzzy logic in renewable energy systems–a review. **Renewable and sustainable energy reviews**, v. 48, p. 585-607, 2015. https://doi.org/10.1016/j.rser.2015.04.037

STORN, R; PRICE, K. Differential evolution–a simple and efficient heuristic for global optimization over continuous spaces. **Journal of global optimization**, v. 11, n. 4, p. 341-359, 1997. https://doi.org/10.1023/A:1008202821328

TAKAGI, T.; SUGENO, M. **Fuzzy identification of systems and its applications to modeling and control.** IEEE Transactions on Systems, Man and Cybernetics, [S.l.], v. 15, n. 1, p. 116-132. 1985. https://doi.org/10.1109/TSMC.1985.6313399

TEIXEIRA, P. C. F. **Comparação de modelos paramétricos e não paramétricos de atuadores com fluido magneto reológico.** Master's thesis. Universidade Federal de Uberlândia, 2017. http://dx.doi.org/10.14393/ufu.di.2017.31

TRUONG, D. Q.; AHN, K. K. MR fluid damper and its application to force sensorless damping control system. **Smart Actuation and Sensing Systems-Recent Advances and Future Challenges, InTech, Rijeka**, p. 383-424, 2012. http://dx.doi.org/10.5772/51391

ZADEH, L. **Fuzzy sets**. Information and control, v. 8, n. 3, p. 338-353, 1965. https://doi.org/10.1016/S0019-9958(65)90241-X